J. Phys. B: At. Mol. Opt. Phys. **30** (1997) 4663–4694. Printed in the UK PII: S0953-4075(97)82346-2

TOPICAL REVIEW

Resonance parameters of photo doubly excited helium

Jan M Rost†, K Schulz‡, M Domke‡ and G Kaindl‡

† Fakultät für Physik, Universität Freiburg, Hermann-Herder-Strasse 3, D-79104 Freiburg, Germany

‡ Institut für Experimentalphysik, Arnimallee 14, D-14195 Berlin, Freie Universität Berlin, Germany

Received 5 March 1997

Abstract. Using theoretical results from complex rotation calculations and data from experimental photoionization cross sections, the quantum defects, the widths, the oscillator strengths and the shape parameter of Rydberg series of autoionizing $^1P^o$ resonances in helium, excited with synchrotron radiation from the ground state, are reviewed and analysed systematically. The relation of these resonance properties to the propensity rules for radiative and non-radiative transitions in two-electron atoms is established.

1. Introduction

Ever since the discovery of strongly correlated two-electron states in early photoabsorption experiments with helium [1] doubly excited states have been in the centre of experimental [2–8] and theoretical [9–18] efforts to understand correlated two-electron dynamics. Recent measurements of photoabsorption [19] as well as electron emission measurements following photoabsorption [20] have reached unprecedented resolution in energy, which has been achieved with a new generation of synchrotron radiation sources and new detector technology. This resolution allows the determination of sensitive details of many resonances beyond their energy position and their widths, namely the Beutler–Fano shape parameter q [21]. Simultaneously, the increasing computing power together with well adapted basis sets for the two-electron Hamiltonian have permitted the *ab initio* calculation of those resonance parameters [8, 18]. The most extensive theoretical studies have concentrated on the $L = 0$ states. For such states the existence of approximate quantum numbers [10, 22] and the existence of propensity rules for autoionization [23] and dipole transitions [13, 24] has been confirmed by high precision calculations [25].

In this study we will discuss resonances of $^1P^o$ symmetry, which are experimentally accessible through photoexcitation from the ground state. The experimental and theoretical determination of the q-parameter is for many resonances still at the limit of technical feasibility. Nevertheless, enough material is now available for a systematic overview of the behaviour of the q-parameter, at least for moderate excitation energies. We will explicitly examine the behaviour of the widths Γ of resonances in the light of the propensity rules for autoionization. Secondly, we will test the propensity rules for photoabsorption looking at the dipole transition probability B^2 into the *bound* part of the resonant wavefunction. We can elucidate the mechanism of dipole absorption in more detail than in previous publications by including the influence of the initial state in the prediction of propensities. Finally, we will relate the behaviour of the q-parameter for individual Rydberg series to the respective quantum numbers and propensity rules. It turns out that the q-parameter is a much more sensitive

0953-4075/97/214663+32$19.50

probe of the dynamics than the resonance positions and even the widths. The increasing sensitivity is easily understood from the nature of these quantities as we will see later.

Within the resonance spectrum, well ordered according to the approximate quantum numbers, we have identified three mechanisms of perturbation whose effects on the resonance parameters are of different strength. The regularity can be perturbed by degeneracies between individual resonance energies from different Rydberg series. A second source of perturbation, setting in at higher energies, comes from the so-called perturber states. Finally, a third but rare source of exceptional behaviour is induced by the morphological similarity of initial- and final-state wavefunctions in the dipole matrix element.

In order to render this paper as self-contained as possible and as such a helpful tool for everybody dealing with doubly excited atomic states, we will summarize some of the concepts and results that are important in the present context. In this spirit we also provide, for future reference, an appendix with tables of our theoretical *ab initio* resonance data of the Rydberg series up to the excitation threshold $N = 7$ of the ion He^+, as far as we have calculated them. In section 2 we review the theoretical basis of the resonance parameters formulated within the concept of complex rotation [26–28]. Rydberg series can be described most elegantly within the quantum-defect theory (QDT) [29], which will be addressed briefly. Section 3 contains a review of the approximate quantum numbers and propensity rules. In section 4 the applicability of the respective propensity rules is critically examined by comparison with the available data that will be discussed for each manifold $N = 2$–7 separately. Section 5 summarizes the results.

2. Theoretical description

2.1. Complex rotation and the photo cross section

In recent years it has become possible to calculate cross sections of two-electron processes with a number of numerical methods. In most of them, e.g. in the R-matrix methods [30–32] or in the hyperspherical close-coupling method [15, 17] as well as in conventional close-coupling methods [33], the cross section is computed on a mesh of energies E. Resonance parameters such as resonance position (E_n), width (Γ_n) and—in photoabsorption—the shape parameter (q_n) are subsequently extracted by a fit in a similar way to that used when these parameters are determined from experimental cross sections.

The method of *complex rotation* [26, 27] is different in that the resonant states are determined directly through diagonalization of a Hamilton matrix [25, 28]. This is possible because the functions of the basis set, containing non-integrable continuum functions to represent the resonant states, are rotated in Hilbert space by complex scaling of the radial coordinates $r \to re^{i\theta}$ in a way that their norm exists and the elements of the Hamilton matrix are well defined. As a consequence, expectation values, or, more precisely, diagonal matrix elements of these complex scaled resonant wavefunctions $|n_\theta\rangle$, are in general complex. This is familiar from the expectation value of the Hamiltonian itself, $\langle n_\theta|H|n_\theta\rangle = E_n - i\Gamma_n/2$, where we are used to interpreting the real part of E_n as the position of the resonance and the imaginary part $\Gamma_n/2$ as its half decay width. However, the expectation values of other operators become complex as well, and their imaginary parts can be used to gain deeper insight into the dynamical details of a system near resonance [34].

Photoabsorption involves the dipole transition probability $P_n = |\langle i|D|n\rangle|^2$ based on the non-diagonal dipole transition matrix element. With the complex rotated resonant state, this *probability* becomes *complex* again at resonance reading [26]

$$D_n^2 \equiv \langle i|D|n_\theta\rangle^2. \tag{1}$$

The squared dipole matrix element is a result of the way in which scalar products are formed with complex rotated wavefunctions [34]. Hence, the familiar formula for the photo cross section, $\sigma(E) = -1/\pi\ \mathrm{Im}\langle i|D^\dagger G(E) D|i\rangle$, reads with complex rotated wavefunctions

$$\sigma(E) = \sigma_0(E) - \frac{1}{\pi}\,\mathrm{Im}\sum_n \frac{\langle i|D|n_\theta\rangle^2}{E - E_n + \mathrm{i}\Gamma_n/2}, \tag{2}$$

where $\sigma_0(E)$ is a smooth background coming from the continuum spectrum of H. Writing real and imaginary parts separately, $\langle i|D|n_\theta\rangle = B_n + \mathrm{i}C_n$, a simple algebraic manipulation transforms (2) into the Fano-shape parametrization of the photo cross section [21],

$$\sigma(E) = \sigma_0(E) + \sum_n \sigma_n(E), \tag{3}$$

where

$$\begin{aligned}
\sigma_n(E) &= \frac{(q_n + \epsilon_n)^2}{1 + \epsilon_n^2}\mu_n^2 - \mu_n^2 \\
\epsilon_n &= \frac{E - E_n}{\Gamma_n/2} \\
q_n &= -\frac{B_n}{C_n} \\
\mu_n^2 &= \frac{2}{\pi\Gamma_n}C_n^2.
\end{aligned} \tag{4}$$

Theoretically, the parameters of (4) are contained in the two matrix elements

$$\begin{aligned}
\langle n_\theta|H|n_\theta\rangle &= E_n - \mathrm{i}\Gamma_n/2 \\
\langle i|D|n_\theta\rangle &= B_n + \mathrm{i}C_n
\end{aligned} \tag{5}$$

of the complex scaled resonant wavefunctions.

To develop a deeper understanding of q_n as the ratio of the real to the imaginary part of the dipole matrix element, we assume for the moment the simple situation of two electrons with principal quantum numbers N and n that interact with the nucleus but not with each other. A doubly excited state $|N, n\rangle$ would not decay but would be degenerate at the same energy $E = E_N + E_n$ with $|N', \epsilon\rangle$ (for simplicity we assume for the moment only one continuum $N' < N$). The electron–electron interaction couples these two states and the doubly excited state becomes a true resonant state with a finite lifetime. Its complex scaled wavefunction at the complex resonance energy reads [34]

$$|n_\theta\rangle = a|N, n\rangle + b|N'\epsilon_\theta\rangle \tag{6}$$

where $|\epsilon_\theta\rangle$ is a (complex scaled) purely outgoing wave. All other wavefunctions as well as the coefficients a, b can be taken as real. If we rearrange the dipole matrix element involving a (real) initial state $|i\rangle$ and the resonant wavefunction as given by (6) according to its real and imaginary parts as in (5), we obtain:

$$B_n = a\langle i|D|N, n\rangle + b\langle i|D|N', \mathrm{Re}(\epsilon_\theta)\rangle \tag{7a}$$

$$C_n = b\langle i|D|N', \mathrm{Im}(\epsilon_\theta)\rangle. \tag{7b}$$

Apart from the small admixture of the (irregular) continuum wavefunction, B_n represents the dipole coupling to the quasibound state $|N, n\rangle$ that is responsible for the resonance. The imaginary part C_n represents the dipole coupling to the continuum. Therefore, we may say that q^2 measures the ratio between the dipole excitation probability to the quasi-bound state and to the continuum at resonance. Very large q^2 values indicate a vanishing continuum coupling, while $q^2 \approx 0$ indicates dominant continuum excitation.

Comparison between experiment and theory is possible for E_n, Γ_n, q_n and, if μ_n^2 is known experimentally, for C_n and B_n. However, the direct experimental determination of μ_n^2 from a fit to the cross section may be severely hampered by a large background. In this case it is easier to calculate the area F_n under a resonance profile σ_n,

$$F_n = \int \sigma_n(E)\mathrm{d}E = \mu_n^2 \frac{\pi\Gamma_n}{2}(q_n^2 - 1) \equiv B_n^2 - C_n^2. \tag{8}$$

The last identity shows that

$$F_n = \mathrm{Re}(D_n^2), \tag{9}$$

in analogy to the definition of an observable from $\mathcal{O} = \mathrm{Re}\langle n_\theta | O | n_\theta \rangle$ from complex rotated wavefunctions. However, (9) does not recover the positive definiteness of a transition probability as it is familiar from square integrable wavefunctions. Negative F_n indicate that the resonance profile appears as a dip, also called a *window resonance*. From (9) it follows, with $|q| < 1$ (i.e. $|B_n| < |C_n|$), that a window resonance has dominant continuum excitation.

In the case of the dipole selection rule, B_n^2 becomes important, which can be expressed as

$$B_n^2 = F_n \frac{q_n^2}{q_n^2 - 1}. \tag{10}$$

2.2. Representation of Rydberg series

In the limit of one electron with principal quantum number $n \gg N$, where N is the principal quantum number of the other electron, we have a Rydberg series for the outer electron almost as in the case of hydrogen. The small perturbation induced by the core electron causes a quantum defect $\delta(E)$, which is a slowly varying function of the energy E and which shifts the energy levels as determined by the condition

$$\tan(\pi[\nu(E) + \delta(E)]) = 0 \tag{11a}$$

$$\nu(E) = \sqrt{\frac{\mathcal{R}}{I_N - E}}, \tag{11b}$$

where $\mathcal{R}$ is the Rydberg constant and I_N is the threshold energy of the excited He^+ ion to which the Rydberg series converges. From the effective quantum number $\nu(E)$, the quantum defect

$$\delta_n = n - \nu_n \tag{12}$$

is defined, where the resonances within a series converging to the threshold N are labelled with increasing energy by $n = n_{\min}, n_{\min} + 1, \ldots$. From (11*a*) it is clear that n is only defined within integer multiples, since the quantum defect is, strictly speaking, only defined modulo 1. We choose $n_{\min}$ for the lowest resonance in each Rydberg series in accordance with the historical independent electron configuration Nl. It permits 'intrashell' configurations $|Nl, n_{\min}l'\rangle + |n_{\min}l', Nl\rangle$ with $n_{\min} = N$ for 'symmetric' states and requires 'intershell' configurations with $n_{\min} = N + 1$ for certain 'asymmetric' states $|Nl, n_{\min}l'\rangle - |n_{\min}l', Nl\rangle$. We define 'symmetric' and 'asymmetric' with respect to the electron exchange in the body-fixed frame, denoted by the quantum number $A = \pm 1$. The definition $n_{\min} = N$ for symmetric states and $n_{\min} = N + 1$ for asymmetric states can be formalized as $n_{\min} = N + (1 - A)/2$. This definition, which provides a smooth dependence of the quantum defect on the quantum number K in each manifold N, only coincides with the historical definition of $n_{\min}$ for $L = 0$ states.

In the framework of QDT multiple Rydberg series which perturb each other can also be treated. However, we do not attempt to describe this theory here, which is well documented

in the original research papers [29] as well as for example in the book by Friedrich [35]. With the help of QDT, we will only motivate the scaling of the resonance parameters from (4) belonging to a given Rydberg series. Condition (11*a*) defines bound-state energies, but it can easily be extended to resonances in the spirit of complex rotation by introducing a complex quantum defect $\delta = \delta_n + \mathrm{i}\delta_I$ in (11*a*). Neglecting terms of order δ_I/ν^2 and smaller, the complex resonance energies fulfilling (11*a*) read as

$$E_n - \mathrm{i}\Gamma_n = I_N - \mathcal{R}\frac{1}{\nu^2} - \mathrm{i}\mathcal{R}\frac{2\delta_I}{\nu^3}. \tag{13}$$

Accordingly, the reduced width $\Gamma_n^*/2 = \Gamma_n\nu^3/2 = \mathcal{R}\delta_I$ should vary slowly along a Rydberg series for $n \to \infty$. Similarly, we may define reduced parameters for photoabsorption that approach a constant value for $n \to \infty$. In summary we describe photoabsorption to Rydberg series with the following reduced quantities:

$$\begin{aligned} &E_n : \delta_n = n - \nu \\ &\Gamma_n : \Gamma_n^* = \Gamma_n\nu^3 \\ &B_n^2 : B_n^{*2} = B_n^2\nu^3 \\ &C_n^2 : C_n^{*2} = C_n^2\nu^3. \end{aligned} \tag{14}$$

From (4) it is clear that the q_n-parameter is already a reduced quantity that will approach a constant value for $n \to \infty$ [36]. This is also true for μ_n^2.

2.3. The molecular approximation

The fact that all the quantities of (14) change smoothly with the excitation ν of the outer electron indicates the possibility of adiabatic approximations. In 1968 Macek [37] introduced the adiabatic hyperspherical approximation to this problem. Lin [38] considerably advanced this approach by showing that one can attach quantum labels to the adiabatic hyperspherical potential curves consistent with the nodal pattern found in numerically computed resonant wavefunctions. Later the hyperspherical treatment was stepwise turned into a quantitative numerical tool for the computation of resonances by Sadeghpour and Greene [13], and more recently by coupling adiabatic hyperspherical channels in the hyperspherical close coupling method [15].

In 1986 Feagin and Briggs introduced another adiabatic approach similar to the Born–Oppenheimer approximation for a diatomic molecule, namely H_2^+, but with reversed roles of electrons and nuclei: for doubly excited states in helium the inter*electronic* axis R is kept fixed to generate adiabatic potential curves $U(R)$ as a function of R. The spatial adiabatic wavefunction is a product of a rotational part $\mathcal{D}_{Mm}^{L,S,t}(\Psi,\Theta,\phi)$, a vibrational part $f_{im}^L(R)$ and a molecular orbital (MO) $\Phi_{im}^t(\rho,z;R)$ (see [14])

$$\Psi_{LM}^{S,t}(\vec{r},\vec{R}) = \mathcal{D}_{Mm}^{L,S,t}(\Psi,\Theta,\phi)\frac{f_{im}^L(R)}{R}\Phi_{im}^t(\rho,z;R), \tag{15}$$

where $(\vec{R},\vec{r})$ are a set of Jacobi coordinates with $\vec{R}$ connecting the two electrons and $\vec{r} = (\rho,z,\phi)$ pointing from the middle of the two electrons to the nucleus. In the body-fixed frame, connected to the laboratory-fixed frame by the Euler angles Ψ,Θ,ϕ, the interelectronic vector $\vec{R}$ is parallel to the z-axis. In contrast to [14] the azimuthal angular dependence on ϕ is described by the rotational wavefunction $\mathcal{D}_{Mm}^{L,S,t}(\Psi,\Theta,\phi)$ and the MO is a wavefunction for the centre-of-mass motion of the nucleus in the coordinates ρ,z at fixed internuclear distance R and for a given quantized azimuthal motion m. The index i counts the quantized states in (ρ,z). The potential for this motion (with $m = 0$) is shown in figure 1.

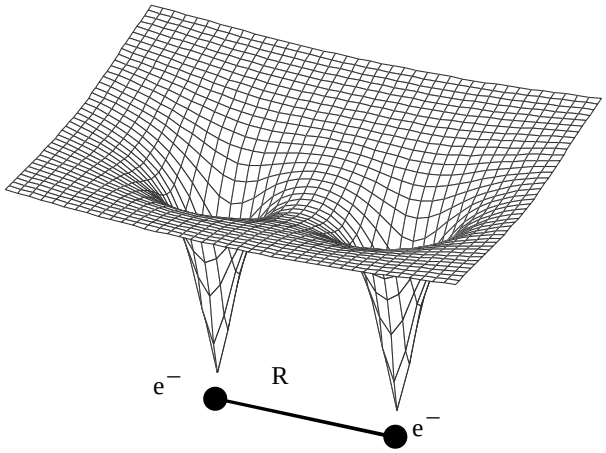

Figure 1. The two-centre Coulomb potential $-2/r_1 - 2/r_2$ is shown at fixed interelectronic distance of 2 au for two-electron motion in helium. The z-axis is parallel to R, the ρ-axis perpendicular to it, see text.

The wavefunction (15) has been constructed to respect all the two-electron symmetries. In particular the rotational part consists of a symmetry adapted linear combination of Wigner D-functions for the Euler angles which transform from a body-fixed to a laboratory-fixed coordinate system,

$$\mathcal{D}^{L,S,t}_{Mm}(\Psi,\Theta,\phi) = D^{L}_{Mm}(\Psi,\Theta,\phi) + (-1)^{S+t+L+m} D^{L}_{M-m}(\Psi,\Theta,\phi). \qquad (16)$$

Hence, the wavefunction (15) is an eigenfunction of the permutation operator P_{12} for the (identical) electrons $P_{12} : \vec{R} \to -\vec{R}, \vec{r} \to \vec{r}$ with eigenvalue $(-1)^S$ where S is the spin of the electron pair, either singlet ($S = 0$) or triplet ($S = 1$). Furthermore, it is an eigenfunction of the parity operator $P : \vec{R} \to -\vec{R}, \vec{r} \to -\vec{r}$ with eigenvalue π and therefore of the product operator PP_{12} with eigenvalue $(-1)^t = (-1)^S\pi$. The remaining quantum number m is the eigenvalue of the projection operator l_z where $\vec{l} = -\mathrm{i}\vec{r} \wedge \nabla_r$ and also of the body-fixed component L_z of the total angular momentum $\vec{L}$.

It can be shown that the wavefunction (15) approximately diagonalizes the two-electron Hamiltonian [14] if its parts are constructed as follows. For fixed R the molecular orbital $\psi^t_{Lm}(\rho, z; R)$ is an eigenfunction of the two-centre Hamiltonian ($Z = 2$ for helium)

$$h_m = -\frac{1}{2}\frac{\partial^2}{\partial z^2} - \frac{1}{2\sqrt{\rho}}\frac{\partial^2}{\partial \rho^2}\sqrt{\rho} - \frac{1}{r_1} - \frac{1}{r_2} + \frac{m^2}{2r^2} \qquad (17)$$

with the Born–Oppenheimer eigenvalue $\mathcal{E}_{im}(R)$. The vibrational wavefunction $f^L_{im}(R)$ is an eigenstate of the adiabatic potential $U^L_{im}(R) = \mathcal{E}_{im}(R) + C^L_{im}(R) + 1/R$, where

$$C^L_{im}(R) = \langle \Phi_{im}| -\frac{\partial^2}{\partial R^2} + \frac{1}{4}\nabla^2_r + \frac{L(L+1) - 2m^2 + \vec{l}^2}{R^2} |\Phi_{im}\rangle \qquad (18)$$

is the expectation value of $H - h_m$, the part of the Hamiltonian not diagonalized by Φ_{im}. Due to the contribution of kinetic energies which enter with different sign in (18) $C(R)$ is small for almost all values of R.

The most important feature of the molecular approximation is the fact that the two-centre

Hamiltonian (17) is separable in prolate spheroidal coordinates [47]

$$\lambda = \frac{r_1 + r_2}{R} \equiv \frac{\sqrt{\rho^2 + (z + R/2)^2} + \sqrt{\rho^2 + (z - R/2)^2}}{R}$$
$$\mu = \frac{r_1 - r_2}{R} \equiv \frac{\sqrt{\rho^2 + (z + R/2)^2} - \sqrt{\rho^2 + (z - R/2)^2}}{R}. \tag{19}$$

The separability implies a product form for the MO with quantum numbers n_λ, n_μ which count the nodes along the respective coordinates,

$$\Phi_{im} = \Lambda^m_{n_\lambda}(\lambda) M^m_{n_\mu}(\mu). \tag{20}$$

Individual resonances are obtained by computing vibrational eigenstates in these potential curves according to the Schrödinger equation

$$\left(-\frac{\partial^2}{\partial R^2} + U^L_{n_\lambda, n_\mu, m}(R) - E_{\bar{n}} \right) f_{\bar{n}}(R) = 0. \tag{21}$$

The vibrational quantum number $\bar{n}$ specifies the excitation of one electron along a Rydberg series where for $\bar{n} \to \infty$ the inner electron remains in an excited He^+ ion. Physically, $\bar{n}$ counts the same states as n in (12) and the relation between both quantum numbers is $\bar{n} = n - N$, where N is the principal quantum number of the $He^+(N)$ hydrogenic level for $\bar{n} \to \infty$. For all distances R of the electrons, or similarly, for any excitation $\bar{n}$ of the outer electron, the state of the inner one and the corresponding potential curve $U(R)$ is defined by the molecular quantum numbers n_λ, n_μ, m. However, in the 'separated atom' limit, when the outer electron has been removed to infinity, it is more convenient to express these quantum numbers in terms of Stark quantum numbers N_1, N_2, m and A for the inner electron in the field of the remote outer electron, where one has directly $N = N_1 + N_2 + m + 1$. Since Stark and molecular quantum numbers are in one-to-one correspondence (see the next section) they are equivalent and we will use the Stark notation in the following since it is closer to other classifications which exist in the literature.

The exact quantum numbers L, M, S, M_S, π and the approximate quantum numbers n, A, N_1, N_2, m constitute a complete classification of doubly excited states. Moreover, they

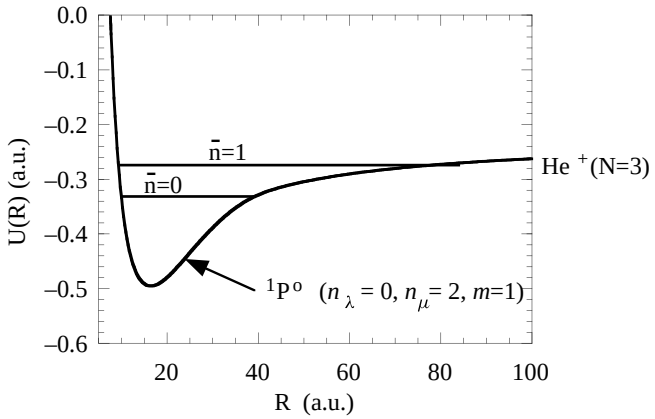

Figure 2. Schematic representation of doubly excited states in helium in an adiabatic approximation. The resonances appear as vibrational eigenstates (the first two are shown) in a potential curve which is constructed from an eigenfunction of all exact symmetries $^{2S+1}L^\pi$ and of the two-centre Coulomb problem with the respective quantum numbers n_λ, n_μ, m, see text. The states $\bar{n}$ form a Rydberg series with the limiting energy of the excited $He^+(N)$ ion for $\bar{n} \to \infty$.

imply an approximate nodal structure of the wavefunctions which in turn leads to propensity rules for radiative transitions involving doubly excited states as well as autoionization. Figure 2 illustrates schematically the calculation of a doubly excited two-electron state with all its quantum numbers in the molecular approximation.

The most recent activity concerning adiabatic approaches to the two-electron problem has led to a merging of the molecular and hyperspherical adiabatic approach with the formulation of so called *hyperspherical elliptic coordinates*. They preserve, to a good extent, the structure of the two-centre molecular Hamiltonian, however, they do not for fixed interelectronic axis R, only for fixed hyper-radius $\mathcal{R}$ [39].

In the next section we will briefly review how the different Rydberg series can be characterized according to the respective approximate quantum numbers of the inner electron, which again remain approximately constant along a given Rydberg series.

3. Approximate quantum numbers and propensity rules

If the two electrons in a two-electron atom moved independently of each other in the field of the nucleus with charge Z, the spectrum would consist of energy levels described by individual quantum numbers nlm and $n'l'm'$. The high degeneracy of the spectrum of two independent electrons is lifted if the electron–electron repulsion is included. Moreover, as a 'good' quantum number (corresponding to an operator that commutes with the Hamiltonian) only the total angular momentum operators L^2 and L_z survive, apart from (trivial) discrete symmetries such as parity and electron exchange as described above (16). These facts have motivated the adiabatic approximations discussed above.

3.1. Approximate classification schemes

Herrick and co-workers [10, 40, 42–44] approached the correlated motion of two electrons from the 'planetary atom' [45] limit where one electron is much further apart from the nucleus than the other, $n_{\text{outer}} \equiv n \gg n_{\text{inner}} \equiv N$. They deduced algebraically several multiplet structures of the resonant states and revealed an approximate set of quantum numbers for the inner electron which are just the Stark quantum numbers $[N_1 N_2 m]$, or in alternative notation ${}_N(K, T)$ with $K = N_2 - N_1$ and $T = m$†. The parabolic quantum numbers characterize the dynamics correctly if the second electron is so far away that it merely creates a (constant) electric field for the inner one. Herrick was surprised that the new classification scheme remained valid even when $n = N$, that is, when both electrons are approximately equally distant from the nucleus [10].

Within the molecular approach as described in section 2.3 Feagin and Briggs [11, 22] later showed that Herrick's classification scheme could be justified with the exact dynamical symmetries (quantum numbers) of the two-centre Coulomb problem, best known from the H_2^+ molecular ion. This dynamical symmetry helped to explain why Herrick's asymptotic quantum numbers ($R \to \infty$) are also valid for smaller R. Moreover, it turned out that the nodal lines corresponding to the prolate spheroidal coordinates λ, μ, φ, in which the two-centre Coulomb problem is separable, are really present in wavefunctions of two-electron resonant states [48]. Recently, Starace and co-workers [41] showed that this remains true even for doubly excited states of multi-electron atoms if the two excited electrons do not interact strongly with the core electrons. The corresponding nodes n_λ, n_μ and m

† The relation to the spherical quantum numbers Nlm is simply $N = N_1 + N_2 + m + 1$, $l = N_2 + m$ and the azimuthal quantum number m is the same. Note that in early textbooks of quantum mechanics $k = -K$ was introduced as 'electric' quantum number in the context of the Stark effect [46].

are uniquely related to the asymptotic (parabolic) classification and to Herrick's quantum numbers through

$$\begin{array}{lcll} \text{Parabolic} & & \text{Molecular} & & \text{Herrick} \\ N_1 & = & n_\lambda & = & \frac{1}{2}(N-K-1-T) \\ N_2 & = & [n_\mu/2] & = & \frac{1}{2}(N+K-1-T) \\ |m| & = & m & = & T \\ A & = & (-1)^{n_\mu} & (=) & A. \end{array} \tag{22}$$

The notation $[x]$ stands for the closest lower integer to x.

Since the information of even and odd nodes n_μ is lost in the parabolic/Herrick's classification, an additional quantum number must be introduced, which has already been given by Herrick [43]. Today it is commonly denoted by A, as coined by Lin who used A as a label to characterize hyperspherical potential curves for two-electron atoms with the values $A = +/-1$ for an antinodal/nodal line of the corresponding adiabatic wavefunctions at $r_1 = r_2$. Lin [38] used the label $A = 0$ for no apparent symmetry with respect to the line $r_1 = r_2$. In the two-centre adiabatic approach, A is indeed the eigenvalue of the *body-fixed* electron exchange operator with values $A = \pm 1$ from $A = (-1)^{n_\mu}$. $A = 0$ does not occur in this description. This is why we put the last equality of (22) in parentheses. The correspondence to a hyperspherical potential curve with the empirical label $A = 0$ would

Table 1. Equivalent quantum numbers for $^1\mathrm{P}^\mathrm{o}$ resonances of helium in the manifolds $N = 1$–7.

Parabolic $[N_1N_2m]^A$	Herrick ${}_N(K,m)^A$	Molecular (n_λ, n_μ, m)	Parabolic $[N_1N_2m]^A$	Herrick ${}_N(K,m)^A$	Molecular (n_λ, n_μ, m)
$[000]^-$	${}_1(0,0)^-$	(0, 1, 0)	$[041]^+$	${}_6(4,1)^+$	(0, 8, 1)
			$[131]^+$	${}_6(2,1)^+$	(1, 6, 1)
$[001]^+$	${}_2(0,1)^+$	(0, 0, 1)	$[221]^+$	${}_6(0,1)^+$	(2, 4, 1)
$[010]^-$	${}_2(1,0)^-$	(0, 3, 0)	$[311]^+$	${}_6(-2,1)^+$	(3, 2, 1)
$[100]^-$	${}_2(-1,0)^0$	(1, 1, 0)	$[401]^+$	${}_6(-4,1)^+$	(4, 0, 1)
			$[050]^-$	${}_6(5,0)^-$	(0, 11, 0)
$[011]^+$	${}_3(1,1)^+$	(0, 2, 1)	$[140]^-$	${}_6(3,0)^-$	(1, 9, 0)
$[101]^+$	${}_3(-1,1)^+$	(1, 0, 1)	$[230]^-$	${}_6(1,0)^-$	(2, 7, 0)
$[020]^-$	${}_3(2,0)^-$	(0, 5, 0)	$[320]^-$	${}_6(-1,0)^-$	(3, 5, 0)
$[110]^-$	${}_3(0,0)^-$	(1, 3, 0)	$[410]^-$	${}_6(-3,0)^-$	(4, 3, 0)
$[200]^-$	${}_3(-2,0)^0$	(2, 1, 0)	$[500]^-$	${}_6(-5,0)^0$	(5, 1, 0)
$[021]^+$	${}_4(2,1)^+$	(0, 4, 1)	$[051]^+$	${}_7(5,1)^+$	(0, 10, 1)
$[111]^+$	${}_4(0,1)^+$	(1, 2, 1)	$[141]^+$	${}_7(3,1)^+$	(1, 8, 1)
$[201]^+$	${}_4(-2,1)^+$	(2, 0, 1)	$[231]^+$	${}_7(1,1)^+$	(2, 6, 1)
$[030]^-$	${}_4(3,0)^-$	(0, 7, 0)	$[321]^+$	${}_7(-1,1)^+$	(3, 4, 1)
$[120]^-$	${}_4(1,0)^-$	(1, 5, 0)	$[411]^+$	${}_7(-3,1)^+$	(4, 2, 1)
$[210]^-$	${}_4(-1,0)^-$	(2, 3, 0)	$[501]^+$	${}_7(-5,1)^+$	(4, 0, 1)
$[300]^-$	${}_4(-3,0)^0$	(3, 1, 0)	$[060]^-$	${}_7(6,0)^-$	(0, 13, 0)
			$[150]^-$	${}_7(4,0)^-$	(1, 11, 0)
$[031]^+$	${}_5(3,1)^+$	(0, 6, 1)	$[240]^-$	${}_7(2,0)^-$	(2, 9, 0)
$[121]^+$	${}_5(1,1)^+$	(1, 4, 1)	$[330]^-$	${}_7(0,0)^-$	(3, 7, 0)
$[211]^+$	${}_5(-1,1)^+$	(2, 2, 1)	$[420]^-$	${}_7(-2,0)^-$	(4, 5, 0)
$[301]^+$	${}_5(-3,1)^+$	(3, 0, 1)	$[510]^-$	${}_7(-4,0)^-$	(5, 3, 0)
$[040]^-$	${}_5(4,0)^-$	(0, 9, 0)	$[600]^-$	${}_7(-6,0)^0$	(6, 1, 0)
$[130]^-$	${}_5(2,0)^-$	(1, 7, 0)			
$[220]^-$	${}_5(0,0)^-$	(2, 5, 0)			
$[310]^-$	${}_5(-2,0)^-$	(3, 3, 0)			
$[400]^-$	${}_5(-4,0)^0$	(4, 1, 0)			

be a linear combination of several molecular potential curves of different symmetry A. All states of the $N = 2$–7 manifolds with their respective quantum numbers are listed in table 1.

On each state $[N_1N_2m]^A$, n_λ, n_μ, m, or ${}_N(K,T)^A$ of the inner electron a whole (Rydberg) series of resonances is built with increasing excitation of the outer electron indicated by its principal quantum number n (see also figure 2). For $n \to \infty$ the two-electron atom is ionized and the He^+ remains in the excited state of the inner electron. To describe the Rydberg series the additional index n can be added so that a correlated two-electron state has the complete classification $[N_1N_2m]^A_n$ or ${}_N(K,m)^A_n$. In the special case of states with $^1P^o$ symmetry (with which we deal here exclusively since this is the symmetry populated by photoabsorption from the $^1S^e$ ground state of helium) we may simplify the notation. As can be easily verified only the combinations $m = 0, A = -1$ and $m = 1, A = +1$ are possible. Hence it is not necessary to specify A explicitly. Moreover, provided only $m = 0, 1$ occur (for $^1P^o$ states) it is not even necessary to state m explicitly if N is known. From $N - K = 2N_1 + m + 1$ follows that $m = 0$ for $N - K$ odd and $m = 1$ for $N - K$ even. Hence, for photoabsorption from the ground state of helium one can use the short notation N, K_n to label resonant states [8]. An equivalent abbreviation for the parabolic classification is N, N_2^A and for the molecular quantum numbers N, n_μ.

Depending on the aspect of two-electron correlation one is interested in one or another set of these equivalent designations of the approximate constants of motion is of advantage. In this paper we will mostly use the parabolic set of quantum numbers $[N_1N_2m]^A$ and the short version N_2^A for states of $^1P^o$ symmetry. It provides all quantum numbers separately and, nevertheless, with $N = N_1 + N_2 + m + 1$, the corresponding N manifold is easily read from this classification. Also, the physical interpretation of $[N_1N_2m]^A$ as the levels of the inner electron in the field of the (distant) outer electron is intuitively clear: nodes in N_1 locate charge density of the inner electron towards the outer one (both electrons are on the same side of the nucleus) while nodes in N_2 indicate that the electrons are located on opposite sides of the nucleus. Finally, the parabolic quantum numbers are in between the (more physical) spheroidal two-centre quantum numbers n_λ, n_μ, m and the (more commonly used) quantum numbers $(K,T)^A$. For the radiative propensity rules yet another combination of the described quantum numbers plays an important role.

3.2. Propensity rules for radiative and non-radiative transitions

3.2.1. Autoionization. The approximate constants of motion for correlated two-electron dynamics imply a nodal structure for the respective resonant states [48]. In turn this nodal structure leads to preferences for autoionization [23]. They are easily understood in the molecular language of adiabatic potential curves for He identified by a set $[N_1N_2m]^A$ of quantum numbers. A small subset of such potential curves as a function of the adiabatic interelectronic distance R is shown in figure 3. The most obvious features in figure 3 are avoided crossings between the two potential curves respectively. Their locus as a function of R (indicated by full squares in figure 3(b)) follows closely the saddle point of the two-centre Coulomb potential that plays a crucial role for the three-body Coulomb problem. The saddle point for fixed R (see figure 1) is defined by $\vec{r}_1 + \vec{r}_2 = 0$, where the $\vec{r}_i$ are the two electron–nucleus vectors.

The avoided crossings may be interpreted in the following way: to the right of such a crossing, the adiabatic two-electron wavefunction has its main contribution in one of the Coulombic wells separated from the other well by a classically forbidden region, with the probability density at the saddle point being small. To the left of the avoided crossing, the wavefunction has its main contribution at the saddle point. Hence, the avoided crossings

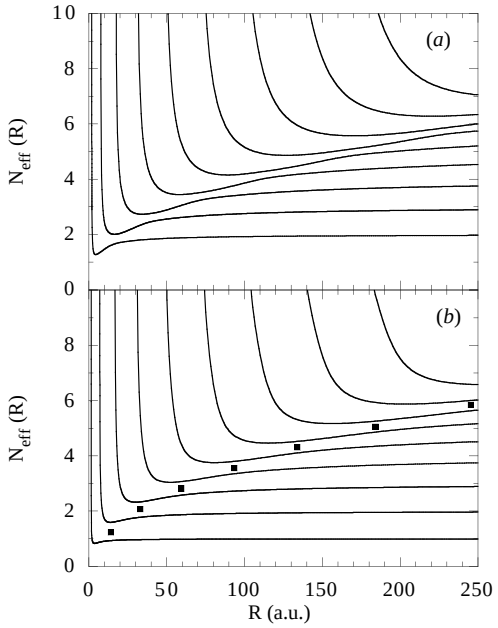

Figure 3. Adiabatic molecular potential curves for two-electron doubly excited states as a function of the interelectronic distance R. The resonances appear as vibrational eigenstates in the potential curves. The energy is plotted as effective quantum number $N(R) = (-2/\epsilon(R))^{1/2}$ with $N(R \to \infty) = 2, 3, 4, \ldots$ indicating directly the $He^+(N)$ ionization thresholds. (*a*) This shows potential curves which carry the resonances of the principal series with quantum numbers $[0, N-1, 1]^+$, $N = 2, \ldots, 10$ from below. (*b*) This shows resonances of $A = -1$ symmetry for $N = 1, \ldots, 9$ corresponding to the quantum numbers $[0, N-1, 0]^-$ from below. To guide the eye the full squares indicate the locus of the avoided crossing, see text.

separate two regions in R in which the wavefunction has different character. As can be seen in figure 3, potential curves whose quantum numbers differ by $\Delta N_2 = 1$ (i.e. $\Delta n_\mu = 2$) display avoided crossings, which are narrower for $A = +1$ states (whose wavefunction has an antinode on the saddle) than for $A = -1$ states (with a node on the saddle, compare figure 3(*a*) with figure 3(*b*)). In the latter case the change in character of the wavefunction as a function of R passing an avoided crossing is not so dramatic, since for reasons of symmetry the wavefunction is zero exactly at the saddle point for all R.

The mechanism of autoionization relies on non-adiabatic transitions in this description, in full analogy to electronic transitions in molecules, as explained in [14, 23]. *Radial* transitions are sensitive to the change of the wavefunction as a function of R. Hence, they occur preferentially through an avoided crossing of two potential curves. The second kind of non-adiabatic transition is due to *rotational* coupling $\Delta m = 1$ between potential curves. Finally, there is no explicit mechanism to change N_1 (n_λ). Hence, decay with $\Delta N_1 \neq 0$ is strongly suppressed. From these observations one can extract three propensity rules for autoionization [23], which are labelled according to the relative efficiency of the underlying decay mechanism:

$$\text{(A)} \qquad \Delta N_2 = -1 \tag{23a}$$

$$\text{(B)} \qquad \Delta m = -1 \tag{23b}$$

$$\text{(C)} \qquad \Delta N_1 \neq 0. \tag{23c}$$

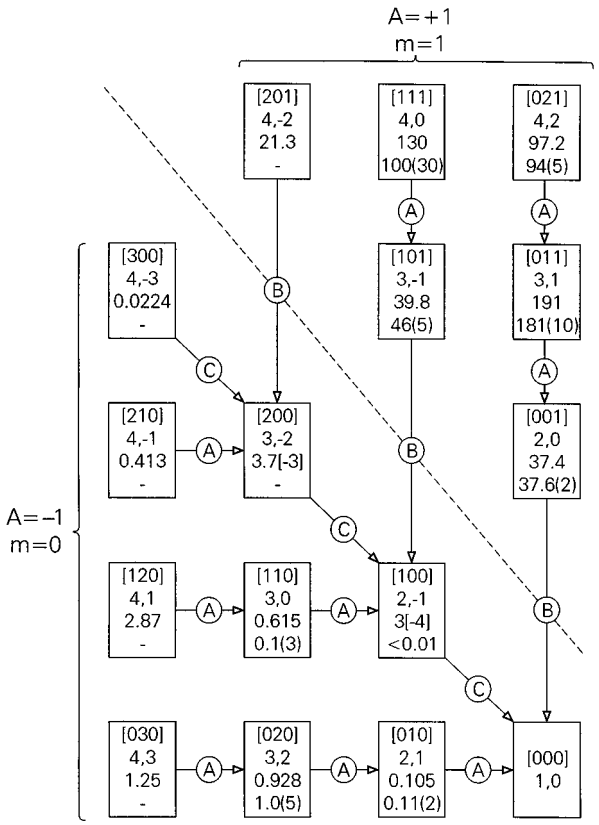

Figure 4. Decay modes indicated by arrows with the respective rule from (16) for the lowest resonances in the manifolds $N = 2$–4. Each box represents a continuum channel and the lowest resonance in this channel where the quantum numbers $[N_1N_2m]$ and N, K are given together with the theoretical and experimental width in meV (uncertainty in parentheses). The diagonal (broken) separates $A = +1$ and $A = -1$ states.

In general, states with $A = +1$ have larger widths than those with $A = -1$. The decay systematics for the lowest resonance $n = N$ in each series $[N_1N_2m]$ is visualized in figure 4. Each box contains the width of the lowest resonance of the respective series with quantum numbers $[N_1N_2m]$. The box also represents the continuum $[N_1N_2m]$ into which a higher lying resonance may decay as indicated by the arrows and the respective mechanism (A), (B) or (C).

In the upper right triangle the states with $A = +1$ are located. Those which can decay according to rule (A) have the largest widths (of the order of 10^2 meV). The arrows point to quantum numbers of the continuum into which these states decay according to rule (A). Close to the (broken) diagonal line separating $A = +1$ and $A = -1$ states we see those resonances that cannot decay by (A). Instead, they decay according to (B) by changing their rotational quantum number. Since this change also implies a change of A, the decay arrow has to cross the diagonal and points to a continuum state with $A = -1$. The rotational decay of these $A = +1$ states is only slightly less effective (by about a factor of 5) than the decay of the $A = +1$ states according to (A). Hence, we combine all $A = +1$ states located in the upper triangle to 'I-class' states with the relatively largest widths.

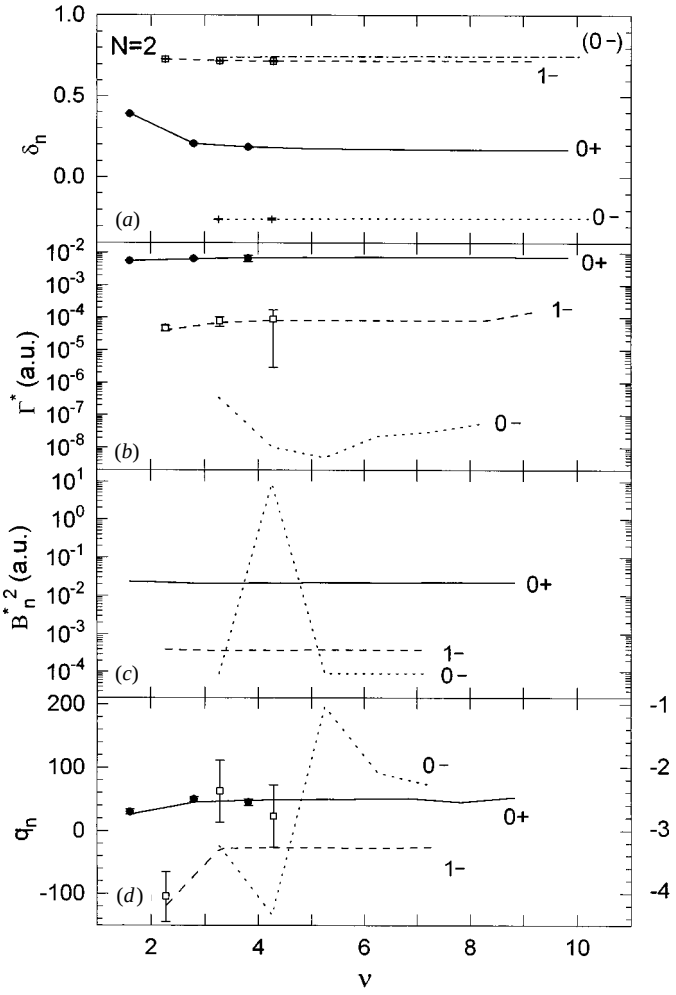

Figure 5. Parameters of resonances in the $N = 2$ manifold; (*a*) quantum defects δ_n, (*b*) reduced widths Γ^*, (*c*) reduced dipole probabilities B^{*2} and (*d*) q-parameter are shown as a function of the effective quantum number ν (11*b*) for photoexcitation from the ground state. The lines connect theoretical values, while the symbols indicate experimental results. Thereby, full lines (full symbols for experimental values) refer to I-class series, broken lines (open symbols) refer to II-class series, and dotted lines (crosses) indicate III-class series. Each series is labelled uniquely by its quantum number N_2^+. The chain lines in (*a*), marked with (N_2^A), show the quantum defect modulo one to highlight almost degenerate energies between resonances of two series. In (*d*) the left scale refers to 0^-, the right scale to 0^+ and 1^-.

The $A = -1$ states below the diagonal that can decay according to (A) define the 'II-class' states. Their widths (of the order of 10^0 meV) are one to two orders of magnitude smaller than the widths of the I-class states. Among the $A = -1$ states are also 'III-class' states located directly below the diagonal. They can only decay according to (C) along the diagonal and their widths (10^{-4}–10^{-2} meV) are more than two orders of magnitude smaller than those of II-class resonances.

To summarize, the propensity rules (A), (B) and (C) group the $^1P^o$ resonant states of helium into three classes I–III with typical widths separated by at least two orders

of magnitude, $\Gamma_{\rm I} : \Gamma_{\rm II} : \Gamma_{\rm III} \approx 10^4 : 10^2 : 1$. Since the propensities depend on the nodal structure $[N_1 N_2 m]$, they should not only hold for the intrashell states $n = N$ as demonstrated in figure 5, but also for entire series characterized by a single $[N_1 N_2 m]$ configuration. III-class states for $^1{\rm P}^{\rm o}$ resonances are restricted to the $[N-1, 0, 0]^-$ configurations, which enforce decay through a $\Delta N_1 \neq 0$ transition (C). The special character of these states is also highlighted in Lin's classification where they are the only $^1{\rm P}^{\rm o}$ states with $A = 0$ (see table 1). To this class belong states of the $[N_1 N_2 m]^A = [100]^-$ Rydberg series, with very small widths as a consequence (figure 5(*b*)). In contrast the I-class series $[001]^+$ has an allowed transition ($\Delta m = -1$, rule (B)) into the (only available) continuum channel $[000]^-$ and the widths are correspondingly large. The $[010]^-$ series is of II-class and has correspondingly smaller widths. Figure 5(*b*) clearly demonstrates the three classes and large differences of the widths between these classes in the $N = 2$ manifold. The widths of the Rydberg series in the manifolds $N = 3$–7 will be discussed in section 4.

3.2.2. Dipole transitions. Propensity rules for radiative transitions can be derived by analysing the dipole matrix elements according to the nodal structure of the resonant wavefunctions, which is a simple analytical task on the potential saddle for $2\vec{r} \equiv \vec{r}_1 + \vec{r}_2 = 0$. This region in configuration space is most relevant for symmetrically excited electrons with $N \approx n$. It corresponds to the equilibrium geometry of a linear ABA molecule [49]. Not surprisingly, the relevant quantum number

$$v_2 = 2N_1 + m \tag{24}$$

for radiative propensities quantizes the two-fold degenerate bending motion of tri-atomic molecules and can be derived by normal mode analysis about the saddle point [14, 24]. Dipole matrix elements within the saddle approximation follow the selection rule

$$\text{(D)} \qquad \Delta v_2 = 0, \pm 1 \tag{25}$$

that survives for the entire dynamics as a propensity rule. Rule (D) has been derived from properties of the doubly excited state involved in the dipole transition. A preference among the possible transitions according to (D) can be induced by the second state of the dipole matrix element. For instance, in radiative *decay* of doubly excited $^1{\rm S}^{\rm e}$ (i.e. $A = +1$) states, rule (D) has been confirmed with a preference for $\Delta v_2 = 0$ transitions [24]. This is because the wavefunction of a true resonant state designated by the approximate quantum numbers $[N_1, N_2, m]^A$ contains an admixture of the channels $[N_1, j, m]^A$ with $j < N_2$. The admixture has the effect that the wavefunction of the doubly excited state has a tail of amplitude at smaller electron–nucleus distances. Hence, it enhances the overlap with spatially less extended (less excited) states. However, the tail is larger for $A = +1$ states than for $A = -1$ states due to larger coupling indicated by the narrower avoided crossings between the $A = +1$ potential curves (see figure 3). Therefore, among the transitions according to (D), a preference exists for the transition which has the least number of avoided crossings between the two states involved in the dipole matrix element, and $A = +1$ for the higher excited state. Hence, there is a preference for $\Delta v_2 = 0$ for radiative decay of $^1{\rm S}^{\rm e}$ (i.e. $A = +1$) states. In this way one could also view the propensity (A) for autoionization.

Here, we are interested in photoabsorption into doubly excited states from the ground state of helium. The final $A = +1$ states with the admixture of lower channels for the relatively best overlap with the ground state can only be $m = +1$ states due to the $^1{\rm P}^{\rm o}$ symmetry. Therefore, we expect a preference for

$$\Delta v_2 = 1 \tag{26}$$

transitions (i.e. $\Delta m = 1$). In each manifold N there is only one series $[0, N-2, 1]^+$ fulfilling this condition. We will call this series the *principal series* as it is commonly referred to in literature.

Propensity rule (D) refers to the bound part B_n^2 (see (7*a*)) of the dipole matrix elements D_n^2. The propensities hold, as for autoionization, for the Rydberg series built on respective configurations $[N_1N_2m]^A$. Figure 5(*c*) shows absorption from the ground state $[000]^+$ into the $N = 2$ manifold. As expected, the principal series $[001]^+$ has the largest $(B^*)^2$ values, those of $[010]^-$ and $[100]^-$, not supported by (26), are much smaller. A systematic overview for higher manifolds N will be given in the next section.

4. Systematics of $^1P^o$ resonances and their propensities in the manifolds $N = 2$–7

In this section, we will analyse the parameters of the Fano parametrization Γ_n, q_n, and also B_n^2 as well as the quantum defect δ_n in their reduced form according to (14) for a large number of Rydberg series. We will check the propensities for autoionization and dipole excitation as described in the previous section and we will also identify three different sources of irregular behaviour. Each subsection highlights one special feature described in the heading. All theoretical data are given in the form of tables in the appendix.

4.1. $N = 2$: almost vanishing decay leads to large fluctuations in q of $[100]^-$

Autoionization and dipole propensities for the $N = 2$ manifold have already been discussed. A closer inspection of the widths of the $[100]^-$ series reveals that they are close to zero around $\nu = 5$. As can be seen from the quantum defects (figure 5(*a*) and table 2), the resonances $[010]_n^-$ and $[100]_{n-1}^-$ (chain) have almost degenerate energies. This leads to strong interference and in turn to almost vanishing widths for some of the $[100]^-$ resonances (figure 5(*b*)). An exact 'bound state in the continuum' with $\Gamma_n = 0$ would imply an infinite

Table 2. Asymptotic quantum defect $[\delta_n], n \to \infty$ modulo one for Rydberg series fitted to complex rotation calculations and experiment. The numbers in parentheses give the uncertainty in the last digits.

N	$[N_1N_2m]$	$[\delta_\infty]$ Theory	$[\delta_\infty]$ Experiment
2	[001]	0.174	0.174(10)
	[010]	0.723	0.719(10)
	[100]	0.750	0.746(15)
3	[011]	0.844	0.85(5)
	[101]	0.748(3)	0.85[a]
	[020]	0.302	0.25
	[110]	0.502(6)	
	[200]	0.407	
4	[021]	—	
	[111]	0.732	0.71(3)
	[201]	0.370(2)	
	[030]	0.859	
	[120]	0.128	
	[210]	0.260(3)	
	[300]	0.028	

[a] Experimentally indistinguishable from δ_∞ of the [011] series.

q_n according to (4). Hence, the very small widths $\Gamma_n \approx 10^{-10}$ au lead to large fluctuations in q_n of the $[100]^-$ series (figure 5(*d*)).

4.2. $N = 3$: interference between $[011]^+$ and $[101]^+$ induces fluctuations in q of $[101]^+$

The widths (figure 6(*b*)) are in perfect agreement with the autoionization propensities: large widths for the I-class series $[011]^+$ and $[101]^+$, smaller widths for the II-class series $[020]^-$ and $[110]^-$, and very small width for the III-class series $[200]^-$ without the preferred decay channel (rule (C)). Behaviour as expected according to the propensities is also found for the dipole transition probability to the bound part of the resonance wavefunction, B_n^2, as shown in figure 6(*c*). The dipole-favoured principal series $[011]^+$ is stronger than all other series. However, the $[101]^+$ series shows rather strong variations in B_n^2 and also in q (figure 6(*d*)). The reason for this is an interaction between the $[011]^+$ and $[101]^+$ series, made possible by similar quantum defects (see the chain line (0^+) in figure 6(*a*) and table 2). Again, as

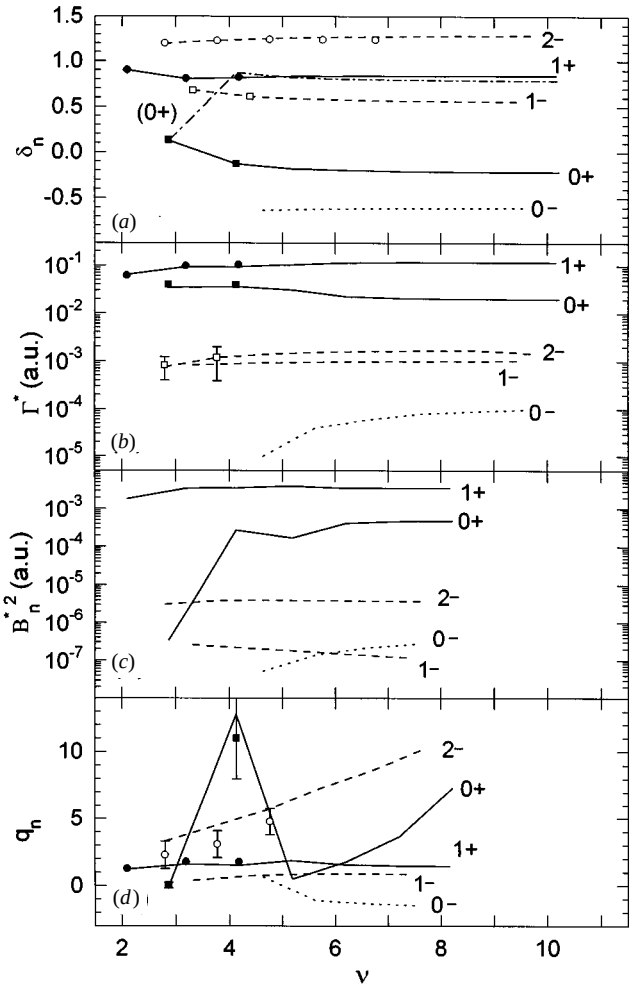

Figure 6. Same quantities as in figure 5 for the five Rydberg series of the $N = 3$ manifold.

in the $N = 2$ manifold, the energetically almost degenerate resonant states belonging to two different Rydberg series interfere leading to the irregular pattern in B_n^2 and q_n. Note that an interference of two Rydberg series with $A = +1$ and $A = -1$ due to their almost degenerate quantum defects cannot occur in the spectra of doubly excited states with angular momentum $L = 0$ most extensively studied by theory.

4.3. $N = 4$: exceptional behaviour of the $[111]^+$ series

Looking first at the widths (figure 7(*b*)), we see a grouping according to the propensities into three blocks, where the first one ($\Gamma^* \approx 5 \times 10^{-2}$ au) contains the I-class series $[021]^+$, $[111]^+$ and $[201]^+$. The second block ($\Gamma^* \approx 5 \times 10^{-3}$ au) is built from the II-class series $[030]^-$, $[120]^-$ and $[210]^-$, and the third group contains the only III-class series $[300]^-$ ($\Gamma^* \approx 5 \times 10^{-5}$ au).

The dipole propensities predict a dominant absorption into the principal series $[021]^+$ which is confirmed by the calculation (figure 7(*c*)). The series $[201]^+$ is strongly modulated.

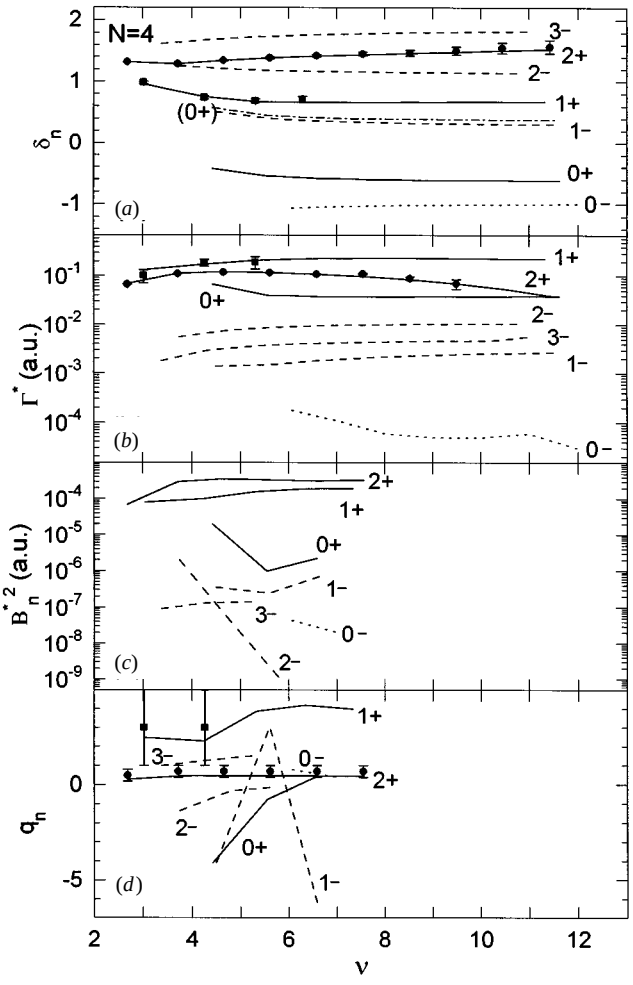

Figure 7. Same quantities as in figure 5 for the seven Rydberg series of the $N = 4$ manifold.

The reason for this is the same mechanism as in $N = 3$ and $N = 2$. Almost degenerate states of different series interfere, namely members of the $[201]^+$ and $[210]^-$ series, as the quantum defects reveal (chain line (0^+) in figure 7(a) and table 2). We also know that these interferences lead to modulations in q for the respective series, which is indeed the case (see q_n for the $[210]^-$ series in figure 7(d)).

However, there is a new, unusual behaviour: The series $[111]^+$ absorbs almost as much oscillator strength as the principal series $[021]^+$. Moreover, $[111]^+$ has the largest widths in the $N = 4$ manifold. The anomaly cannot be explained with the interference mechanism introduced so far. It is a very special case, where the resonant wavefunction $[111]^+$ has a character similar to that of the ground-state wavefunction of helium: the respective charge densities have an almost isotropic angular distribution denoted by the same correlation quantum numbers $K = N_2 - N_1 = 0$ and $A = +1$ for both states. An overlap that is larger than with other wavefunctions in the same manifold $N = 4$ is the consequence. This large overlap results in comparatively large widths for the members of the $[111]^+$ series and an enhanced ability to absorb light from the ground state. Note that it is important that K and A of the initial and final state coincide. For $[110]^-$ e.g. K is also zero but $A = -1$, and the series behaves regularly. Note that B_n^2 as well as q_n are very sensitive, and we have only obtained converged numerical values for a few resonances of the weaker Rydberg series of class II and III.

4.4. $N = 5$: the effect of perturber states

So far we have dealt with Rydberg series whose irregularities were caused by interactions with resonances belonging to other Rydberg series of the same manifold N or by properties of the initial state. In the $N = 5$ manifold, the influence of a so called *perturber* or *intruder* becomes visible. A perturber is a state that belongs from its quantum numbers to a Rydberg series of a higher manifold, e.g. in the present case to $N = 6$. However, its energy E_n is so low that it lies below the energy of a lower threshold, here $N = 5$. Hence, energetically, this state can perturb all the series of the $N = 5$ manifold. However, according to the mechanism which also leads to the autoionization propensities, Rydberg series which differ by $\Delta N_2 = \pm 1$ are most strongly coupled (through avoided crossings), which means that a perturber with quantum numbers $[N_1 N_2 m]^A$ has the strongest influence on the series $[N_1, N_2 - 1, m]^A$. The perturber state itself no longer exists as a true resonance. Instead, the perturbed Rydberg series contains one state more leading to a jump of the quantum defect near the energy of the perturber [50]. If this jump is unity, the perturber state is entirely absorbed into the respective Rydberg series. This is almost the case in the $N = 5$ manifold indicating how effective the coupling mechanism of the avoided crossings is, since energetically the perturber state could influence all the series in the $N = 5$ manifold and not just the one to which it is connected by $\Delta N_2 \pm 1$. In the energy range of figure 8(a) we have one perturber state from $[041]^+$ which leads to a jump of the quantum defect for $[031]^+$ around $\nu = 7$. The second perturber from $[131]^+$ induces a jump in δ_n for the $[121]^+$ series. The corresponding reduced widths (figure 8(b)) also show a modulation near the location of the perturbers. A position and width can be assigned to a perturber state by analytically detuning the basis-set for the diagonalization so that the perturbed Rydberg series remains unresolved. Numerical results for the perturber states obtained in this way are labelled by 'PT' in the tables in the appendix.

Otherwise, the widths are still regular enough to recognize the familiar pattern of the three classes. The four series of I-class have widths approximately larger by a factor of 10 than the four series of II-class, whose widths in turn are an order of magnitude larger than

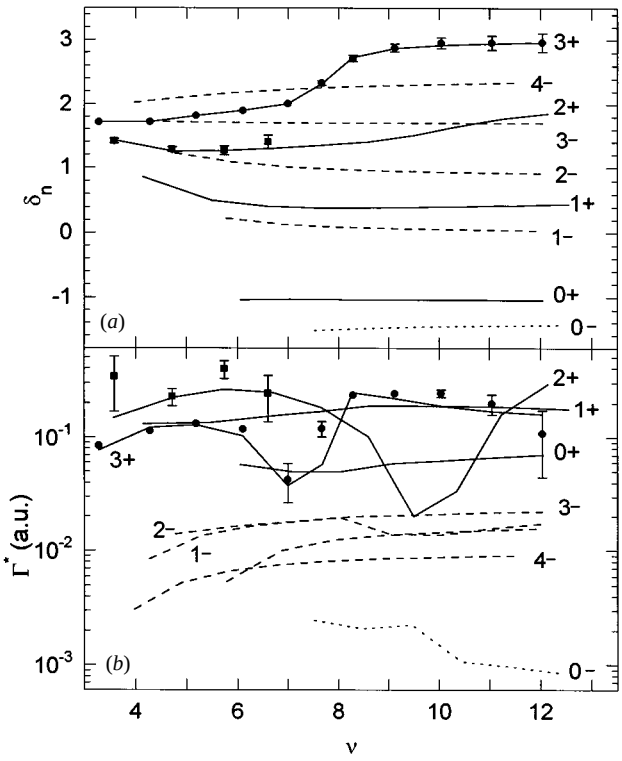

Figure 8. Quantum defects δ_n (*a*), and reduced widths $\Gamma^*/2$ (*b*), for the nine Rydberg series of the $N = 5$ manifold. The data are coded as in figure 5.

those of the III-class series $[400]^-$. Note, however, that the reduced widths of the three classes are much less separated (by a factor of 10) than in the $N = 3$ manifold (by a factor of 100). This is a sign of the increasing instability of the resonances and the increasing number of possible decay channels.

It is not surprising that the dipole excitation probabilities B^2, which are more sensitive to details of the dynamics than the widths, show very large variations over seven orders of magnitude (see table A4 in the appendix). Note that ${B^*}_n{}^2$ of the principal series $[031]^+$ is strongly modulated in the vicinity of the perturber. Overall, the absolute values of ${B^*}_n{}^2$ have already become quite small as compared with the $N = 2$ manifold.

4.5. $N = 6, 7$: the beginning loss of propensities

As can be seen in figures 9 and 10, the resonances of $N = 6$ and $N = 7$ are no longer clearly organized in well separated series for $\nu < 20$. This indicates the beginning of a loss of approximate quantum numbers and consequently of propensities. The $N = 6$ manifold contains 11 Rydberg series, seven of them have assimilated a total number of nine perturber states from higher manifolds. In the $N = 7$ manifold, 18 perturber states have been assimilated by 10 out of 13 Rydberg series. In both cases, only some of the perturbers are visible in figures 9 and 10. These numbers show two facts. Firstly, more and more Rydberg series become perturbed, 63% in the $N = 6$ manifold, and 77% in the $N = 7$ manifold which demonstrates the loss of approximate quantum numbers. Secondly, the perturbers

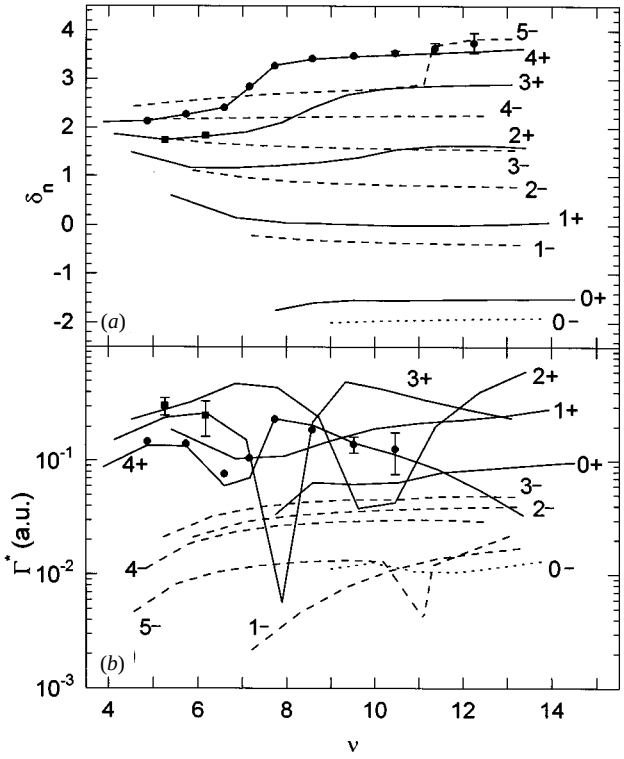

Figure 9. Same quantities as in figure 8 for the 11 Rydberg series of the $N = 6$ manifold.

influence only selected Rydberg series, namely those to which they are connected by a quantum number difference of $\Delta N_2 = 1$. This shows that the mechanism which controls the coupling between channels $[N_1 N_2 m]^A$ and which is responsible for the propensity rules (see section 3.2) is still operative.

For increasingly higher excitation, even this rule seems to break down, since a perturber state couples to more than one Rydberg series, as indicated by a jump of less than unity in the quantum defect of a single Rydberg series due to a perturber. However, there is an alternative and consistent interpretation of this observation: very high-lying Rydberg series are composed of several pure $[N_1 N_2 m]^A$ 'channels' which reflect the loss of the approximate quantum numbers. Assuming that a perturber with quantum numbers $[N_1 N_2 m]^A$ connects only to the component which fulfils $\Delta N_2 = 1$, one can conclude that all Rydberg series which are perturbed by the specific perturber contain the $[N_1, N_2 - 1, m]^A$ channel. This interpretation has been worked out up to much higher manifolds for $^1\mathrm{S}^\mathrm{e}$ states of helium in [25]. The $^1\mathrm{P}^\mathrm{o}$ resonances are different from the $^1\mathrm{S}^\mathrm{e}$ states since $A = +1$ and $A = -1$ states are not separated by an exact symmetry. However, for the manifolds $N = 2$–7 discussed here, all the propensity rules and quantum numbers have been demonstrated to hold to the same accuracy as in the case of S symmetry.

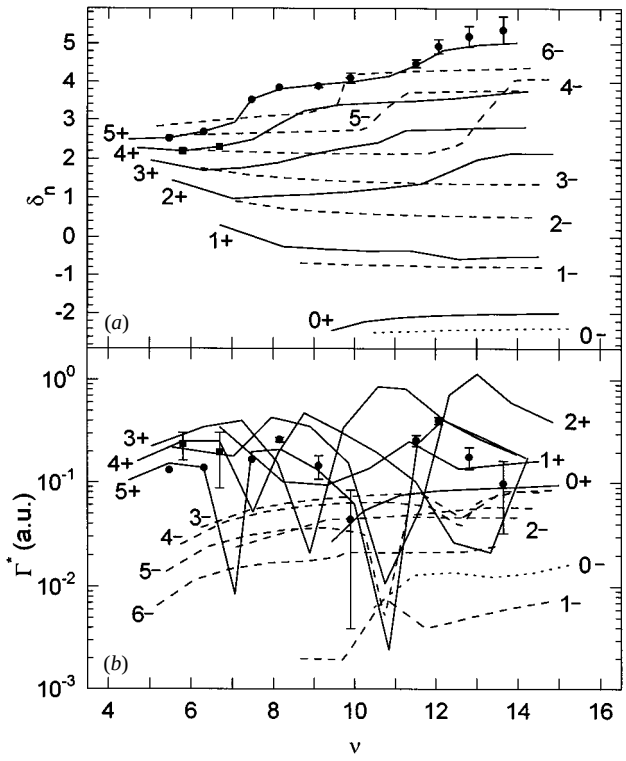

Figure 10. Same quantities as in figure 8 for the 13 Rydberg series of the $N = 7$ manifold. The extremely small width ($\Gamma^* = 2.9955 \times 10^{-5}$ au) of the $[060]^-_{13}$ state at $\nu = 9.586\,55$ is not shown.

5. Summary

We can summarize that helium resonances, photoexcited from the ground state, are organized in regular series roughly up to the $N = 5$ threshold of He^+. The mechanisms, which cause limited violations of the propensity rules for autoionization and for dipole absorption, are (i) interference of $A = +1$ and $A = -1$ channels within one manifold N due to similar quantum defects δ_n, (ii) morphological similarity of the resonant wavefunction with the initial-state wavefunction, expressed by identical correlation quantum numbers $K = N_1 - N_2 = 0$ and $A = +1$, and finally (iii) the perturber states which begin to dissolve the regular spectrum starting in the $N = 5$ manifold. Furthermore, we may group the quantities that are relevant to photoabsorption according to their sensitivities on details of the dynamics. The sensitivities follow from the nature of the quantities and can clearly be seen by comparing the presented figures. Least sensitive is the energy position E_n as the *real* part of a *diagonal* matrix element. More sensitive is the width Γ_n as the *imaginary* part of a diagonal matrix element, followed by B_n which is the *real* part of an *off-diagonal* matrix element. The most sensitive parameter in photoabsorption is q_n, which is the *ratio* of the real and imaginary part of an *off-diagonal* matrix element. If in the future even higher resonance data should become available, both experimentally and theoretically, we will see if a mixing between $A = \pm 1$ has a significant effect on the spectrum at higher energies. Furthermore, it will be

very interesting to monitor experimentally with ultrahigh resolution the loss of the regular resonant structure for higher excitations N and to observe and analyse a qualitatively new regime of overlapping resonances [51–53]. This regime will coexist with regular tails of Rydberg series which should prevail for planetary configurations $n \gg N \gg 1$ and might open a completely new perspective on highly correlated electron dynamics.

Acknowledgments

This work would not have been possible without Dieter Wintgen's input. He lead the numerical part of this project before his tragic death in August 1994. JMR acknowledges gratefully support by the Deutsche Forschungsgemeinschaft (DFG) within the SFB 276 located at Freiburg University and under the Gerhard Hess-program. The work in Berlin was supported by the DFG, project Do 560/1-1.

Appendix

In the appendix we list theoretical parameters of helium $^1P^o$ resonances converging to the thresholds $N = 2$–7. Similar tables for $^1S^e$ resonances can be found in [25].

Table A1. Theoretical resonance parameter as defined in section 2 in atomic units converged to the given digits, 7.698e–05 stands for 7.698×10^{-05}.

N, K $[N_1 N_2 m]^A$	n	$-E$	$\Gamma/2$	ν	Γ^*	$(B^*)^2$	q
2, 0	2	0.693 134 920	6.866 25e–04	1.6090	5.7202e–03	2.38e–02	−2.77
$[001]^+$	3	0.564 085 188	1.505 94e–04	2.7932	6.5638e–03	2.10e–02	−2.58
	4	0.534 363 144	6.417 3e–05	3.8145	7.1235e–03	2.15e–02	−2.55
	5	0.521 504 666	3.289 8e–05	4.8219	7.3766e–03	2.17e–02	−2.54
	6	0.514 733 994	1.899 8e–05	5.8254	7.5112e–03	2.19e–02	−2.53
	7	0.510 726 795	1.192 6e–05	6.8273	7.5906e–03	2.19e–02	−2.52
	8	0.508 158 54	7.96e–06	7.8285	7.6380e–03	2.25e–02	−2.58
	9	0.506 413 84	5.59e–06	8.8293	7.6952e–03	2.24e–02	−2.5
	10	0.505 175	4e–06	9.829	7.5966e–03		
2, 1	3	0.597 073 804	1.923e–06	2.2695	4.4958e–05	4.00e–04	−4.25
$[010]^-$	4	0.546 493 257	1.014e–06	3.2794	7.1522e–05	3.67e–04	−3.32
	5	0.527 297 770	4.91e–07	4.2798	7.6980e–05	3.83e–04	−3.31
	6	0.517 937 328	2.67e–07	5.2797	7.8589e–05	3.88e–04	−3.31
	7	0.512 679 987	1.60e–07	6.2795	7.9237e–05	3.89e–04	−3.32
	8	0.509 435 853	1.03e–07	7.2794	7.9460e–05	3.94e–04	−3.3
	9	0.507 294 315	6.8e–08	8.2793	7.7182e–05		
	10	0.505 806 96	1.0e–07	9.2792	1.5979e–04		
2, −1	3	0.547 092 709	5e–09	3.2584	3.4596e–07	9.29e–05	−23.4
$[100]^-$	4	0.527 616 338	7e–11	4.2550	1.0785e–08	8.75e + 00	−133
	5	0.518 118 268	1.7e–11	5.2532	4.9290e–09	8.66e–05	197
	6	0.512 791 034	4.7e–11	6.2522	2.2973e–08	8.66e–05	91
	7	0.509 508 462	4e–11	7.2515	3.0506e–08	8.65e–05	72
	8	0.507 344 240	5e–11	8.2511	5.6174e–08		
	9	0.505 842 69		9.2509			
	10	0.504 759 0		10.250			

Table A2. Theoretical resonance parameter defined as in table A1.

N, K $[N_1N_2m]^A$	n	$-E$	$\Gamma/2$	ν	Γ^*	$(B^*)^2$	q
3, 1	3	0.335 625 935	3.511 869e–03	2.0990	6.4955e–02	1.82e–03	1.25
$[011]^+$	4	0.271 193 403	1.448 131e–03	3.1943	9.4397e–02	3.47e–03	1.64
	5	0.250 773 561	6.500 18e–04	4.1840	9.5218e–02	3.64e–03	1.53
	6	0.240 948 845	3.810 19e–04	5.1664	1.0508e–01	4.02e–03	1.88
	7	0.235 381 267	2.459 01e–04	6.1633	1.1514e–01	3.56e–03	1.58
	8	0.231 969 855	1.602 66e–04	7.1613	1.1772e–01	3.54e–03	1.50
	9	0.229 730 760	1.091 06e–04	8.1597	1.1855e–01	3.56e–03	1.47
	10	0.228 182 57	7.734e–05	9.1584	1.1882e–01		
	11	0.227 068	5.6e–05	10.157	1.1736e–01		
3, −1	3	0.282 828 970	7.310 40e–04	2.8721	3.4639e–02	3.50e–07	0.04
$[101]^+$	4	0.251 578 561	2.600 89e–04	4.1269	3.6561e–02	2.68e–04	12.8
	5	0.240 848 064	1.117 98e–04	5.1811	3.1098e–02	1.66e–04	0.52
	6	0.235 242 888	4.802 2e–05	6.1968	2.2854e–02	4.18e–04	1.80
	7	0.231 855 536	2.817 0e–05	7.2044	2.1067e–02	4.74e–04	3.67
	8	0.229 642 356	1.860 8e–05	8.2088	2.0586e–02	4.88e–04	7.33
	9	0.228 114 738	1.309 8e–05	9.2116	2.0476e–02		
	10	0.227 015 3	9.5e–06	10.2135	2.0243e–02		
3, 2	4	0.285 950 743	1.704 6e–05	2.8010	7.4921e–04	3.12e–06	3.33
$[020]^-$	5	0.257 432 288	1.101 7e–05	3.7683	1.1791e–03	4.00e–06	4.52
	6	0.244 412 373	6.559e–06	4.7468	1.4031e–03	4.07e–06	5.74
	7	0.237 433 023	4.058e–06	5.7334	1.5296e–03	4.00e–06	7.35
	8	0.233 279 233	2.642e–06	6.7246	1.6068e–03	3.87e–06	8.68
	9	0.230 614 628	1.801e–06	7.7187	1.6564e–03	3.78e–06	10.3
	10	0.228 806 184	1.278e–06	8.7145	1.6916e–03		
	11	0.227 523 8	8e–07	9.7114	1.4654e–03		
3, 0	4	0.267 644 001	1.134e–05	3.3178	8.2833e–04	2.61e–07	0.44
$[110]^-$	5	0.248 224 394	5.362e–06	4.3851	9.0427e–04	2.10e–07	0.77
	6	0.239 292 313	2.997e–06	5.4121	9.5021e–04	1.73e–07	0.90
	7	0.234 331 075	1.844e–06	6.4259	9.7857e–04	1.43e–07	0.92
	8	0.231 269 832	1.213e–06	7.4339	9.9665e–04	1.20e–07	0.89
	9	0.229 242 993	8.39e–07	8.4390	1.0085e–03		
	10	0.227 830 076	6.04e–07	9.4425	1.0170e–03		
3, −2	4	0.245 517 652	6.8e–08	4.6329	1.3523e–05	5.26e–08	0.69
$[200]^-$	5	0.238 061 744	1.06e–07	5.6184	3.7599e–05	1.38e–07	−1.09
	6	0.233 663 277	1.02e–07	6.6108	5.8937e–05	2.18e–07	−1.33
	7	0.230 864 587	8.6e–08	7.6062	7.5689e–05	2.82e–07	−1.46
	8	0.228 977 474	6.9e–08	8.6033	8.7876e–05		
	9	0.227 646 123	5.5e–08	9.6013	9.7360e–05		

Table A3. Theoretical resonance parameter defined as in table A1.

N, K $[N_1N_2m]^A$	n	$-E$	$\Gamma/2$	ν	Γ^*	$(B^*)^2$	q
4, 2	4	0.194 512 131	1.787 174e–03	2.6813	6.8903e–02	6.77e–05	0.29
$[021]^+$	5	0.161 251 205	1.083 9e–03	3.7126	1.1093e–01	2.99e–04	0.47
	6	0.148 049 432	6.031 97e–04	4.6563	1.2179e–01	3.64e–04	0.49
	7	0.140 850 169	3.322 16e–04	5.6156	1.1766e–01	3.43e–04	0.48

Table A3. (Continued)

N, K $[N_1N_2m]^A$	n	$-E$	$\Gamma/2$	ν	Γ^*	$(B^*)^2$	q
	8	0.136 528 961	1.910 47e–04	6.5848	1.0909e–01	3.15e–04	0.48
	9	0.133 746 663	1.136 64e–04	7.5602	9.8234e–02	3.44e–04	0.47
	10	0.131 859 129	6.817 1e–05	8.5376	8.4846e–02		
	11	0.130 522 475	4.084 2e–05	9.5150	7.0366e–02		
	12	0.129 542 54	2.388e–05	10.4914	5.5152e–02		
	13	0.128 803 4	1.31e–05	11.4656	3.9490e–02		
4, 0	4	0.178 798 722	2.386 550e–03	3.0463	1.3494e–01	7.69e–05	2.47
$[111]^+$	5	0.152 734 009	1.131 881e–03	4.2433	1.7296e–01	9.99e–05	2.29
	6	0.142 629 121	7.033 36e–04	5.3224	2.1209e–01	1.64e–04	3.88
	7	0.137 451 388	4.505 29e–04	6.3338	2.2895e–01	1.85e–04	4.20
	8	0.134 288 843	2.984 27e–04	7.3339	2.3544e–01	2e–04	4
	9	0.132 200 330	2.046 58e–04	8.3306	2.3664e–01		
	10	0.130 745 628	1.449 73e–04	9.3264	2.3521e–01		
	11	0.129 691 063	1.057 07e–04	10.3221	2.3251e–01		
	12	0.128 902 07	7.904e–05	11.3180	2.2919e–01		
4, −2	4	0.150 557 131	3.908 74e–04	4.4227	6.7630e–02	2.26e–05	−4.09
$[201]^+$	5	0.141 252 456	1.177 07e–04	5.5465	4.0168e–02	9.79e–07	−0.75
	6	0.136 539 778	6.697 4e–05	6.5823	3.8201e–02	2.19e–06	0.47
	7	0.133 661 140	4.268 2e–05	7.5979	3.7442e–02		
	8	0.131 750 537	2.968 2e–05	8.6062	3.7841e–02		
	9	0.130 412 715	2.149 3e–05	9.6111	3.8164e–02		
	10	0.129 438 038	1.605 8e–05	10.6142	3.8405e–02		
	11	0.128 705 43	1.231e–05	11.6162	3.8590e–02		
4, 3	5	0.168 846 093	2.306 0e–05	3.3769	1.7760e–03	9.30e–08	1.00
$[030]^-$	6	0.151 832 846	1.833 9e–05	4.3167	2.9503e–03	1.35e–07	1.28
	7	0.142 992 362	1.241 1e–05	5.2716	3.6363e–03	1.42e–07	1.53
	8	0.137 840 402	8.336e–06	6.2402	4.0511e–03		
	9	0.134 596 793	5.737e–06	7.2181	4.3150e–03		
	10	0.132 432 020	4.069e–06	8.2022	4.4907e–03		
	11	0.130 919 534	2.970e–06	9.1905	4.6112e–03		
	12	0.129 823 09	2.23e–06	10.1817	4.7076e–03		
	13	0.129 003 9	2.1e–06	11.175	5.8613e–03		
4, 1	5	0.160 689 529	5.271 8e–05	3.7429	5.5288e–03	1.98e–06	−1.35
$[120]^-$	6	0.146 733 780	3.534 5e–05	4.7964	7.8003e–03	4.19e–08	−0.30
	7	0.139 754 471	2.278 9e–05	5.8213	8.9913e–03	1e–09	−0.07
	8	0.135 701 425	1.513 9e–05	6.8354	9.6698e–03		
	9	0.133 126 050	1.045 5e–05	7.8441	1.0092e–02		
	10	0.131 383 962	7.481e–06	8.8499	1.0371e–02		
	11	0.130 149 302	5.519e–06	9.8540	1.0561e–02		
	12	0.129 241 900	4.178e–06	10.8569	1.0693e–02		
4, −1	5	0.149 763 990	7.594e–06	4.4934	1.3779e–03	3.56e–07	−4.07
$[210]^-$	6	0.140 969 138	4.243e–06	5.5956	1.4867e–03	2.45e–07	3.05
	7	0.136 349 933	3.129e–06	6.6372	1.8298e–03	7e–07	−6.7
	8	0.133 523 369	2.348e–06	7.6591	2.1099e–03		
	9	0.131 648 243	1.780e–06	8.6722	2.3219e–03		
	10	0.130 335 158	1.368e–06	9.6808	2.4823e–03		
	11	0.129 378 050	1.068e–06	10.6867	2.6070e–03		
	12	0.128 658 20	8.5e–07	11.6910	2.7165e–03		

Table A3. (Continued)

N, K $[N_1N_2m]^A$	n	$-E$	$\Gamma/2$	ν	Γ^*	$(B^*)^2$	q
4, −3	5	0.138 613 869	4.12e–07	6.0603	1.8340e–04	4.40e–08	0.81
$[300]^-$	6	0.135 102 260	1.54e–07	7.0352	1.0725e–04	2e–08	0.4
	7	0.132 774 213	5.9e–08	8.0197	6.0863e–05		
	8	0.131 159 886	3.2e–08	9.0095	4.6803e–05		
	9	0.129 997 623	2.5e–08	10.0024	5.0036e–05		
	10	0.129 134 285	2.3e–08	10.9973	6.1180e–05		
	11	0.128 476 02	1e–08	11.9934	3.4503e–05		

Table A4. Theoretical resonance parameter defined as in table A1.

N, K $[N_1N_2m]^A$	n	$-E$	$\Gamma/2$	ν	Γ^*	$(B^*)^2$	q
5, 3	5	0.126 398 689	1.088 654e–03	3.2820	7.6975e–02	1.51e–05	−0.207
$[031]^+$	6	0.107 287 651	7.807 76e–04	4.2793	1.2237e–01	3.59e–07	−0.022
	7	0.098 616 265	4.622 87e–04	5.1813	1.2861e–01	2.93e–08	−0.006
	8	0.093 446 374	2.279 96e–04	6.0973	1.0336e–01	2.34e–08	0.006
	9	0.090 235 128	5.550 5e–05	6.9893	3.7902e–02	9.88e–07	0.067
	10	0.088 491 985	6.458 8e–05	7.6731	5.8357e–02	9.25e–05	0.538
	11	0.087 300 171	2.184 46e–04	8.2732	2.4740e–01	6.65e–05	0.190
	12	0.085 995 647	1.447 35e–04	9.1300	2.2030e–01	3.55e–06	0.046
	13	0.084 918 985	9.209 8e–05	10.0807	1.8869e–01	6e–07	0.02
	14	0.084 091 661	6.289 4e–05	11.0534	1.6987e–01		
	15	0.083 452	4.6e–05	12.034	1.6033e–01		
5, 1	5	0.119 233 456	1.628 873e–03	3.5676	1.4793e–01	8.9e–06	0.44
$[121]^+$	6	0.102 150 534	1.052 069e–03	4.7471	2.2509e–01	3.69e–05	0.71
	7	0.095 189 318	7.002 04e–04	5.7328	2.6385e–01	4.67e–05	0.70
	8	0.091 137 537	4.131 42e–04	6.6968	2.4816e–01	4.09e–05	0.63
	9	0.088 537 716	2.050 50e–04	7.6510	1.8368e–01	8.39e–06	0.24
	10	0.086 770 197	7.998 1e–05	8.5933	1.0151e–01	2.20e–05	0.99
	11	0.085 550 431	1.181 4e–05	9.4912	2.0202e–02	1.6e–06	0.7
	12	0.084 669 506	1.532 4e–05	10.3478	3.3958e–02		
	13	0.083 966 869	5.684 2e–05	11.2261	1.6084e–01		
	14	0.083 389 54	8.250e–05	12.1428	2.9542e–01		
5, −1	5	0.109 097 499	9.209 79e–04	4.1438	1.3106e–01	4.54e–06	−29
$[211]^+$	6	0.096 547 358	4.072 84e–04	5.4957	1.3521e–01	2.95e–06	1.93
	7	0.091 523 508	2.681 69e–04	6.5857	1.5320e–01	4.50e–06	1.88
	8	0.088 632 704	1.913 07e–04	7.6091	1.6856e–01	8.03e–07	0.40
	9	0.086 748 626	1.489 13e–04	8.6059	1.8983e–01		
	10	0.085 427 964	1.074 06e–04	9.5963	1.8983e–01		
	11	0.084 463 776	7.968 9e–05	10.5823	1.8887e–01		
	12	0.083 737 043	5.968 8e–05	11.5659	1.8470e–01		
	13	0.083 175 01	4.498e–05	12.5482	1.7774e–01		
5,-3	5	0.093 685 604	1.311 90e–04	6.0442	5.7936e–02	1.38e–07	0.68
$[301]^+$	6	0.090 127 327	7.251 7e–05	7.0263	5.0310e–02	1.03e–06	2.38
	7	0.087 751 551	4.825 6e–05	8.0313	4.9996e–02	1.42e–07	−0.34
	8	0.086 123 429	3.985 1e–05	9.0361	5.8805e–02		
	9	0.084 961 197	3.086 8e–05	10.0389	6.2459e–02		
	10	0.084 102 891	2.477 1e–05	11.0391	6.6646e–02		
	11	0.083 449 134	2.020 1e–05	12.0399	7.0514e–02		

Table A4. (Continued)

N, K $[N_1N_2m]^A$	n	$-E$	$\Gamma/2$	ν	Γ^*	$(B^*)^2$	q
5, 4	6	0.111 743 628	2.475 4e–05	3.9688	3.0949e–03	1.27e–09	0.24
$[040]^-$	7	0.100 909 544	2.257 9e–05	4.8900	5.2805e–03	3.28e–09	0.41
	8	0.094 736 906	1.682 2e–05	5.8248	6.6489e–03	4.57e–09	0.59
	9	0.090 891 352	1.208 4e–05	6.7755	7.5175e–03	8.16e–09	0.70
	10	0.088 348 875	8.796e–06	7.7387	8.1532e–03	3.4e–11	−0.01
	11	0.086 589 702	6.417e–06	8.7107	8.4824e–03		
	12	0.085 325 948	4.808e–06	9.6892	8.7469e–03		
	13	0.084 389 840	3.674e–06	10.6724	8.9320e–03		
	14	0.083 678 30	2.87e–06	11.6590	9.0970e–03		
5, 2	6	0.107 476 720	5.452 5e–05	4.2658	8.4651e–03	5.54e–07	1.50
$[130]^-$	7	0.097 887 683	4.569 8e–05	5.2870	1.3507e–02	5.98e–08	−1.06
	8	0.092 629 436	3.307 3e–05	6.2920	1.6477e–02	2.61e–02	0.12
	9	0.089 399 031	2.358 2e–05	7.2936	1.8299e–02	3.84e–09	−0.13
	10	0.087 268 098	1.7562e–05	8.2942	2.0041e–02		
	11	0.085 788 056	1.2761e–05	9.2943	2.0491e–02		
	12	0.084 718 712	9.738e–06	10.2937	2.1243e–02		
	13	0.083 919 479	7.597e–06	11.2946	2.1892e–02		
	14	0.083 307 9	6.0e–06	12.2944	2.2300e–02		
5, 0	6	0.101 938 432	6.4196e–05	4.7740	1.3969e–02	8.38e–08	−2.86
$[220]^-$	7	0.094 300 364	3.9374e–05	5.9130	1.6281e–02	1.54e–08	−0.78
	8	0.090 252 625	2.6141e–05	6.9834	1.7805e–02	2.64e–09	0.50
	9	0.087 764 354	1.9031e–05	8.0247	1.9669e–02	1.8e–07	6.02
	10	0.086 107 301	9.328e–06	9.0482	1.3820e–02		
	11	0.084 938 504	6.758e–06	10.0621	1.3769e–02		
	12	0.084 078 611	5.837e–06	11.0721	1.5845e–02		
	13	0.083 426 24	4.92e–06	12.0802	1.7347e–02		
5, −2	6	0.095 008 763	1.4040e–05	5.7718	5.3993e–03	5.11e–09	31.6
$[310]^-$	7	0.090 610 992	1.5508e–05	6.8645	1.0032e–02	4.31e–09	−1.67
	8	0.088 002 165	1.2546e–05	7.9046	1.2393e–02	2.58e–09	1.45
	9	0.086 273 922	9.620e–06	8.9272	1.3688e–02		
	10	0.085 059 034	7.385e–06	9.9415	1.4512e–02		
	11	0.084 169 144	5.772e–06	10.9512	1.5161e–02		
	12	0.083 496 539	4.592e–06	11.9582	1.5705e–02		
5, −4	6	0.088 845 250	2.921e–06	7.5185	2.4829e–03	9.47e–08	6.43
$[400]^-$	7	0.086 939 055	1.712e–06	8.4886	2.0943e–03	1.6e–08	1.9
	8	0.085 578 293	1.323e–06	9.4675	2.2454e–03		
	9	0.084 576 520	4.70e–07	10.4524	1.0734e–03		
	10	0.083 819 758	3.21e–07	11.4411	9.6147e–04		
	11	0.083 234 874	2.21e–07	12.4324	8.4936e–04		

Table A5. Theoretical resonance parameter defined as in table A1. Perturber states as explained in section 4.4 are denoted by 'PT'.

N, K $[N_1N_2m]^A$	n	$-E$	$\Gamma/2$	ν	Γ^*	$(B^*)^2$	q
6, 4	6	0.088 602 8	7.465e–04	3.888 99	8.7815e–02	PT	
$[041]^+$	7	0.076 648 564	5.930 82e–04	4.867 29	1.3677e–01	6.72e–05	−0.45
	8	0.070 757 965	3.576 64e–04	5.733 75	1.3484e–01	6.15e–05	−0.42

Table A5. (Continued)

N, K $[N_1N_2m]^A$	n	$-E$	$\Gamma/2$	ν	Γ^*	$(B^*)^2$	q
	9	0.067 072 296	1.053 57e–04	6.588 80	6.0272e–02	1.68e–05	−0.33
	10	0.065 291 914	9.617 7e–05	7.165 90	7.0780e–02	2.21e–07	−0.030
	11	0.063 941 556	2.571 44e–04	7.718 88	2.3652e–01	6.89e–05	−0.29
	12	0.062 332 268	1.633 81e–04	8.587 78	2.0695e–01	4.48e–07	−0.020
	13	0.061 052 043	8.333 8e–05	9.536 85	1.4457e–01	3.60e–10	−0.4
	14	0.060 095 673	4.905 4e–05	10.493 79	1.1337e–01		
	15	0.059 365 36	2.801e–05	11.455 79	8.4221e–02		
	16	0.058 798 5	1.43e–05	12.417 0	5.4754e–02		
	17	0.058 356	7e–06	13.363	3.3407e–02		
6, 2	6	0.084 824 59	1.083 47e–03	4.131 02	1.5276e–01	PT	
$[131]^+$	7	0.073 645 119	8.293 97e–04	5.253 26	2.4048e–01	1.2e–07	0.04
	8	0.068 622 411	5.568 81e–04	6.181 64	2.6309e–01	1.5e–07	0.04
	9	0.065 512 641	2.168 89e–04	7.085 03	1.5427e–01	4.39e–06	−0.23
	10	0.063 587 132	5.808e–06	7.890 14	5.7057e–03	4.94e–07	−0.96
	11	0.062 334 868	1.744 21e–04	8.585 87	2.2079e–01	6.08e–04	8.6
	12	0.061 285 986	3.052 29e–04	9.331 04	4.9596e–01	1.63e–05	0.27
	13	0.060 358 493	2.015 16e–04	10.196 36	4.2724e–01		
	14	0.059 576 796	1.240 23e–04	11.146 8	3.4354e–01		
	15	0.058 957 54	7.993e–05	12.120 7	2.8466e–01		
	16	0.058 467 3	5.33e–05	13.102	2.3976e–01		
6, 0	6	0.079 999 302	1.255 933e–03	4.518 27	2.3169e–01	PT	
$[221]^+$	7	0.070 199 995	8.265 31e–04	5.836 21	3.2861e–01	2.23e–06	1.38
	8	0.066 203 931	7.436 63e–04	6.839 92	4.7595e–01		
	9	0.063 773 028	4.661 95e–04	7.790 99	4.4094e–01		
	10	0.062 119 713	1.853 24e–04	8.725 01	2.4618e–01		
	11	0.060 956 027	2.151 9e–05	9.622 03	3.8340e–02		
	12	0.060 128 380	1.886 4e–05	10.456 57	4.3135e–02		
	13	0.059 415 603	6.905 3e–05	11.379 85	2.0353e–01		
	14	0.058 823 15	1.060 8e–04	12.365 14	4.0111e–01		
	15	0.058 3329	1.265e–04	13.407	6.0970e–01		
6, −2	6	0.072 692 534	6.022 13e–04	5.399 04	1.8955e–01		
$[311]^+$	7	0.066 231 347	1.619 97e–04	6.843 01	1.0382e–01		
	8	0.063 474 312	1.098 33e–04	7.945 57	1.1019e–01		
	9	0.061 773 868	1.039 57e–04	8.966 09	1.4986e–01		
	10	0.060 564 586	9.685 7e–05	9.989 58	1.9311e–01		
	11	0.059 686 733	8.151 5e–05	10.999 8	2.1698e–01		
	12	0.059 031 037	6.708 5e–05	11.992 7	2.3142e–01		
	13	0.058 527 57	5.759e–05	12.968 77	2.5123e–01		
	14	0.058 132	5.3e–05	13.929	2.8646e–01		
6, −4	6	0.063 897 456	3.637 0e–05	7.741 93	3.3754e–02		
$[401]^+$	7	0.062 332 355	5.076 7e–05	8.589 41	6.4343e–02		
	8	0.061 057 904	3.601 5e–05	9.532 44	6.2392e–02		
	9	0.060 057 477	2.767 2e–05	10.538 53	6.4775e–02		
	10	0.059 321 103	2.593 4e–05	11.522 94	7.9358e–02		
	11	0.058 747 779	2.1710e–05	12.515 00	8.5110e–02		
	12	0.058 295 45	1.859e–05	13.508 61	9.1652e–02		
	13	0.057 933	1.6e–05	14.502	9.7596e–02		

Table A5. (Continued)

N, K $[N_1N_2m]^A$	n	$-E$	$\Gamma/2$	ν	Γ^*	$(B^*)^2$	q
6, 5	7	0.079 515 759	2.4694e–05	4.568 14	4.7080e–03		
[050]$^-$	8	0.072 223 314	2.4771e–05	5.477 04	8.1398e–03		
	9	0.067 779 451	1.9827e–05	6.395 58	1.0374e–02		
	10	0.064 861 167	1.5003e–05	7.330 14	1.1818e–02		
	11	0.062 851 836	1.1216e–05	8.278 16	1.2725e–02		
	12	0.061 416 692	8.381e–06	9.236 21	1.3207e–02		
	13	0.060 361 885	6.141e–06	10.199 48	1.3032e–02		
	14	0.059 606 94	1.51e–06	11.109 21	4.1405e–03		
	15	0.059 459 34	4.13e–06	11.317 27	1.1973e–02		
	16	0.058 929 3	4.5e–06	12.173 8	1.6238e–02		
	17	0.058 449	5e–06	13.146	2.2719e–02		
6, 3	7	0.077 020 444	4.9639e–05	4.826 36	1.1161e–02		
[140]$^-$	8	0.070 308 609	4.7446e–05	5.821 60	1.8722e–02		
	9	0.066 351 579	3.7352e–05	6.805 36	2.3545e–02		
	10	0.063 793 922	2.8314e–05	7.790 45	2.6774e–02		
	11	0.062 044 175	2.1189e–05	8.778 23	2.8666e–02		
	12	0.060 796 106	1.5990e–05	9.767 76	2.9803e–02		
	13	0.059 875 541	1.2173e–05	10.758 27	3.0315e–02		
	14	0.059 177 745	9.349e–06	11.748 93	3.0324e–02		
	15	0.058 638 2	7.0e–06	12.735 8	2.8921e–02		
6, 1	7	0.073 892 177	7.4210e–05	5.221 83	2.1133e–02		
[230]$^-$	8	0.068 065 139	6.4580e–05	6.322 07	3.2637e–02		
	9	0.064 750 545	4.9026e–05	7.374 03	3.9316e–02		
	10	0.062 631 764	3.6535e–05	8.405 83	4.3399e–02		
	11	0.061 181 674	2.7280e–05	9.427 07	4.5709e–02		
	12	0.060 143 275	2.0009e–05	10.439 59	4.5531e–02		
	13	0.059 367 776	1.6197e–05	11.452 31	4.8657e–02		
	14	0.058 776 356	1.2689e–05	12.459 50	4.9086e–02		
	15	0.058 313 5	9.9e–06	13.465	4.8338e–02		
6, −1	7	0.069 975 284	5.1741e–05	5.888 50	2.1129e–02		
[320]$^-$	8	0.065 657 455	4.1590e–05	7.035 27	2.8964e–02		
	9	0.063 153 276	3.0859e–05	8.112 24	3.2948e–02		
	10	0.061 521 397	2.3124e–05	9.154 75	3.5484e–02		
	11	0.060 379 345	1.7615e–05	10.180 96	3.7177e–02		
	12	0.059 542 663	1.3648e–05	11.198 35	3.8332e–02		
	13	0.058 909 058	1.0748e–05	12.210 52	3.9135e–02		
	14	0.058 416 74	8.59e–06	13.219 37	3.9688e–02		
6, −3	7	0.065 179 472	2.907e–06	7.207 91	2.1772e–03		
[410]$^-$	8	0.062 833 968	4.059e–06	8.288 32	4.6222e–03		
	9	0.061 301 429	4.726e–06	9.328 39	7.6726e–03		
	10	0.060 221 156	4.856e–06	10.352 16	1.0775e–02		
	11	0.059 424 516	4.633e–06	11.368 09	1.3613e–02		
	12	0.058 818 481	4.095e–06	12.378 87	1.5536e–02		
	13	0.058 345 72	3.60e–06	13.386 6	1.7272e–02		
6, −5	7	0.061 734 162	7.671e–06	8.995 79	1.1169e–02		
[500]$^-$	8	0.060 593 300	6.363e–06	9.962 46	1.2583e–02		
	9	0.059 735 205	4.050e–06	10.937 42	1.0598e–02		
	10	0.059 075 368	3.092e–06	11.918 60	1.0470e–02		
	11	0.058 558 161	2.715e–06	12.904 34	1.1668e–02		
	12	0.058 145 65	2.48e–06	13.894 001	1.3303e–02		

Table A6. Theoretical resonance parameter defined as in table A1.

N, K $[N_1N_2m]^A$	n	$-E$	$\Gamma/2$	ν	Γ^*	$(B^*)^2$	q
7, 5	7	0.065 509	5.76e–04	4.499	1.0491e–01	PT	
$[051]^+$	8	0.057 541 82	4.715 7e–04	5.465 96	1.5402e–01	PT	
	9	0.053 403 165	2.791 57e–04	6.301 54	1.3971e–01	1.04e–04	−0.91
	10	0.050 846 476	1.203 0e–05	7.060 43	8.4682e–03	3.63e–06	−0.92
	11	0.049 772 857	2.400 87e–04	7.469 61	2.0012e–01	1.17e–04	−0.62
	12	0.048 273 635	1.924 02e–04	8.186 26	2.1110e–01	1.57e–04	−0.90
	13	0.046 881 956	8.924 8e–05	9.078 45	1.3356e–01	9.52e–05	−0.84
	14	0.045 826 586	3.133 3e–05	9.989 61	6.2471e–02		
	15	0.045 069 341	9.619 999e–07	10.842 68	2.4525e–03		
	16	0.044 568 703	7.859 3e–05	11.541 45	2.4165e–01		
	17	0.044 189 63	1.153 7e–04	12.169 3	4.1583e–01		
	18	0.043 762 6	6.21e–05	13.025 1	2.7445e–01		
	19	0.043 377	3.5e–05	13.972	1.9093e–01		
7, 3	7	0.063 276	7.75e–04	4.714	1.6237e–01	PT	
$[141]^+$	8	0.055 640 773	6.529 96e–04	5.803 37	2.5526e–01	1.00e–04	−0.50
	9	0.051 999 577	4.317 76e–04	6.682 80	2.5773e–01	1.56e–05	−0.52
	10	0.049 698 068	6.131 9e–05	7.502 88	5.1798e–02	1.97e–07	−0.10
	11	0.048 398 011	1.848 52e–04	8.119 05	1.9787e–01	2.68e–06	−0.33
	12	0.047 315 073	3.554 56e–04	8.761 61	4.7815e–01	1.19e–05	−0.29
	13	0.046 226 671	1.821 88e–04	9.609 22	3.2331e–01		
	14	0.045 308 782	8.440 8e–05	10.548 38	1.9814e–01		
	15	0.044 598 224	3.3557e–05	11.497 87	1.0202e–01		
	16	0.044 050 636	6.928e–06	12.433 50	2.6633e–02		
	17	0.043 628 29	4.49e–06	13.334 60	2.1292e–02		
	18	0.043 283 2	3.07e–05	14.236	1.7715e–01		
7, 1	7	0.060 473 4	8.900e–04	5.039 6	2.2783e–01	PT	
$[231]^+$	8	0.053 382 783	6.979 38e–04	6.300 53	3.4912e–01		1.6
	9	0.050 346 398	5.320 24e–04	7.234 86	4.0295e–01		1.6
	10	0.048 436 998	1.492 33e–04	8.098 90	1.5855e–01		1.7
	11	0.047 144 965	1.497 7e–05	8.888 51	2.1035e–02		1.7
	12	0.046 103 722	1.880 36e–04	9.719 82	3.4534e–01		1.7
	13	0.045 265 429	3.629 85e–04	10.574 71	8.5847e–01		1.7
	14	0.044 741 749	2.866 90e–04	11.263 56	8.1935e–01		1.7
	15	0.044 150 384	1.094 74e–04	12.241 17	4.0161e–01		
	16	0.043 685 458	5.923 8e–05	13.198 98	2.7243e–01		
	17	0.043 302 86	3.116e–05	14.179 5	1.7767e–01		
7, −1	7	0.057 027 662	6.473 05e–04	5.550 3	2.2135e–01		
$[321]^+$	8	0.050 951 085	2.607 09e–04	7.022 16	1.8055e–01		1.4
	9	0.048 701 167	4.291 66e–04	7.954 39	4.3199e–01		1.4
	10	0.047 111 742	2.516 84e–04	8.906 62	3.5565e–01		1.5
	11	0.045 976 755	8.197 6e–05	9.842 40	1.5632e–01		1.6
	12	0.045 147 690	4.336e–06	10.744 16	1.0756e–02		
	13	0.044 510 533	1.864 0e–05	11.633 76	5.8700e–02		
	14	0.044 099 816	1.922 33e–04	12.324 24	7.1968e–01		1.6
	15	0.043 752 832	2.599 28e–04	13.010 65	1.1449e+00		1.6
	16	0.043 420 702	1.140 93e–04	13.845 89	6.0569e–01		
	17	0.043 082 4	6.04e–05	14.850 4	3.9562e–01		

Table A6. (Continued)

N, K $[N_1N_2m]^A$	n	$-E$	$\Gamma/2$	ν	Γ^*	$(B^*)^2$	q
7, −3	7	0.051 934 994	5.814 27e–04	6.699 06	3.4960e–01		1.2
$[411]^+$	8	0.048 177 509	9.085 8e–05	8.241 12	1.0171e–01		1.4
	9	0.046 584 530	5.866 0e–05	9.309 96	9.4671e–02		1.5
	10	0.045 477 218	6.200 0e–05	10.356 71	1.3775e–01		1.4
	11	0.044 702 926	8.759 7e–05	11.340 11	2.5549e–01		1.5
	12	0.043 983 281	3.449 5e–05	12.564 49	1.3684e–01		1.7
	13	0.043 552 663	3.040 1e–05	13.517 00	1.5016e–01		
	14	0.043 196 604	2.691 2e–05	14.492 73	1.6384e–01		
7, −5	7	0.046 430 995	1.623 0e–05	9.436 73	2.7278e–02		1.2
$[501]^+$	8	0.045 608 223	2.508 6e–05	10.214 73	5.3474e–02		1.4
	9	0.044 867 976	2.737 0e–05	11.108 66	7.5039e–02		1.5
	10	0.044 260 825	2.392e–05	12.047 98	8.3663e–02		
	11	0.043 768 404	1.984 3e–05	13.014 09	8.7474e–02		
	12	0.043 369 211	1.653 9e–05	13.994 67	9.0662e–02		
	13	0.043 043 64	1.410e–05	14.982 61	9.4844e–02		
7, 6	8	0.059 511 072	2.391 5e–05	5.171 60	6.6157e–03	PT	
$[060]^-$	9	0.054 376 728	2.572 2e–05	6.072 23	1.1518e–02		
	10	0.051 085 674	2.174 0e–05	6.977 71	1.4772e–02		
	11	0.048 832 517	1.705 9e–05	7.897 69	1.6807e–02		
	12	0.047 230 682	1.273 7e–05	8.828 93	1.7532e–02		
	13	0.046 256 910	1.7e–08	9.586 55	2.9955e–05		
	14	0.046 007 995	1.136 6e–05	9.813 65	2.1485e–02		
	15	0.045 145 907	8.509e–06	10.746 36	2.1120e–02		
	16	0.044 464 425	6.678e–06	11.707 15	2.1430e–02		
	17	0.043 928 3	5.3e–06	12.675 6	2.1588e–02		
	18	0.043 502	5e–06	13.65	2.5433e–02		
7, 4	8	0.057 930 646	4.417 1e–05	5.405 10	1.3950e–02		
$[150]^-$	9	0.053 095 634	4.622 8e–05	6.381 10	2.4023e–02		
	10	0.050 082 739	3.886 3e–05	7.345 58	3.0807e–02		
	11	0.048 050 964	3.052 0e–05	8.313 30	3.5070e–02		
	12	0.046 617 513	2.312 1e–05	9.283 76	3.7001e–02		
	13	0.045 582 296	1.515 6e–05	10.242 54	3.2571e–02		
	14	0.045 160 140	2.090e–06	10.728 76	5.1621e–03		
	15	0.044 742 758	1.630 2e–05	11.284 52	4.6851e–02		
	16	0.044 146 533	1.251 5e–05	12.253 13	4.6047e–02		
	17	0.043 669 73	9.93e–06	13.239	4.6083e–02		
	18	0.043 287	8e–06	14.226	4.6065e–02		
7, 2	8	0.056 006 139	6.742 0e–05	5.737 27	2.5464e–02		
$[240]^-$	9	0.051 607 785	6.633 6e–05	6.806 73	4.1840e–02		
	10	0.048 956 548	5.473 0e–05	7.837 17	5.2691e–02		
	11	0.047 195 603	4.288 0e–05	8.853 03	5.9506e–02		
	12	0.045 957 794	3.329 2e–05	9.861 31	6.3852e–02		
	13	0.045 053 447	2.524 3e–05	10.862 85	6.4715e–02		
	14	0.044 380 808	1.768 2e–05	11.843 57	5.8750e–02		
	15	0.043 958 694	9.343e–06	12.614 06	3.7504e–02		
	16	0.043 762 163	1.496 1e–05	13.027 96	6.6164e–02		
	18	0.043 393 04	1.516e–05	13.929 84	8.1954e–02		
	19	0.043 064	1.3e–05	14.916	8.6284e–02		

Table A6. (Continued)

N, K $[N_1N_2m]^A$	n	$-E$	$\Gamma/2$	ν	Γ^*	$(B^*)^2$	q
7, 0	8	0.053 654 151	7.6293e–05	6.240 70	3.7086e–02		
$[330]^-$	9	0.049 908 783	6.6335e–05	7.415 42	5.4098e–02		
	10	0.047 726 990	5.2432e–05	8.505 81	6.4532e–02		
	11	0.046 288 081	4.0820e–05	9.559 00	7.1308e–02		
	12	0.045 272 791	3.2084e–05	10.592 08	7.6254e–02		
	13	0.044 523 737	2.5438e–05	11.612 93	7.9678e–02		
	14	0.043 948 045	1.1356e–05	12.635 47	4.5817e–02		
	15	0.043 506 179	1.6224e–05	13.633 74	8.2231e–02		
	16	0.043 151 33	1.301e–05	14.633 1	8.1530e–02		
7, −2	8	0.050 781 353	3.3743e–05	7.083 44	2.3985e–02		
$[420]^-$	9	0.048 126 949	2.9262e–05	8.269 99	3.3102e–02		
	10	0.046 531 975	2.6966e–05	9.352 95	4.4126e–02		
	11	0.045 436 240	2.0352e–05	10.403 15	4.5828e–02		
	12	0.044 642 517	1.6391e–05	11.431 38	4.8970e–02		
	13	0.044 038 062	1.3957e–05	12.457 68	5.3968e–02		
	14	0.043 570 979	1.1850e–05	13.472 51	5.7955e–02		
	15	0.043 200 258	9.257e–06	14.482 24	5.6235e–02		
7, −4		0.047 465 145	1.519e–06	8.671 87	1.9812e–03		
$[620]^-$	9	0.046 118 172	1.059e–06	9.711 17	1.9397e–03		
	10	0.045 160 758	3.186e–06	10.727 99	7.8674e–03		
	11	0.044 434 270	1.224e–06	11.755 85	3.9772e–03		
	12	0.043 883 227	1.202e–06	12.768 36	5.0043e–03		
	13	0.043 450 804	1.186e–06	13.776 46	6.2019e–03		
	14	0.043 104 559	1.129e–06	14.782 06	7.2934e–03		
7, −6	8	0.045 366 336	2.763e–06	10.482 84	6.3657e–03		
$[600]^-$	9	0.044 626 424	4.312e–06	11.455 57	1.2965e–02		
	10	0.044 056 650	3.576e–06	12.421 97	1.3709e–02		
	11	0.043 601 101	2.570e–06	13.399 54	1.2366e–02		
	12	0.043 233 831	2.285e–06	14.381 40	1.3593e–02		
	13	0.042 933 72	2.33e–06	15.366 81	1.6910e–02		

The values for E, $\Gamma/2$, and q are numerically converged to the digits shown. All data are in atomic units; energies are measured against the double ionization threshold I_∞ at $E = 0$. From the theoretical resonance positions E, the photon energies at which the resonances appear are obtained as

$$E_{\mathrm{exp}}[\mathrm{eV}] = I_\infty - 2\mathcal{R}_{\mathrm{He}}E[\mathrm{au}],$$

with the Rydberg constant $\mathcal{R}_{\mathrm{He}} = 13.603\,83$ eV au^{-1} and the double ionization threshold of $I_\infty = 79.0052$ eV.

References

[1] Madden R P and Codling K 1963 *Phys. Rev. Lett.* **10** 516
[2] Kossmann H, Krässig B and Schmidt V 1988 *J. Phys. B: At. Mol. Opt. Phys.* **21** 1489
[3] Woodruff P R and Samson J A R 1982 *Phys. Rev.* A **25** 848
[4] Zubek M, King G C, Rutter P M and Read F H 1989 *J. Phys. B: At. Mol. Opt. Phys.* **22** 3411

[5] Domke M, Xue C, Puschmann A, Mandel T, Hudson E, Shirley D A, Kaindl G, Greene C H, Sadeghpour H R and Petersen H 1991 *Phys. Rev. Lett.* **66** 1306
[6] Domke M, Remmers G and Kaindl G 1992 *Phys. Rev. Lett.* **69** 1171
[7] Domke M, Schulz K, Remmers G, Gutiérrez A, Kaindl G and Wintgen D 1995 *Phys. Rev.* A **51** R4309
[8] Domke M, Schulz K, Remmers G, Kaindl G and Wintgen D 1996 *Phys. Rev.* A **53** 1424
[9] Fano U 1983 *Rep. Prog. Phys.* **46** 97
[10] Herrick D E 1983 *Adv. Chem. Phys.* **52** 1
[11] Feagin J M and Briggs J S 1986 *Phys. Rev. Lett.* **57** 984
[12] Lin C D 1986 *Adv. At. Mol. Phys.* **22** 77
[13] Sadeghpour H R and Greene C H 1990 *Phys. Rev. Lett.* **65** 313
[14] Rost J M and Briggs J S 1991 *J. Phys. B: At. Mol. Opt. Phys.* **24** 4293
[15] Tang J-Z, Watanabe S, Matsuzawa M and Lin C D 1992 *Phys. Rev. Lett.* **69** 1633
[16] Tang J-Z, Watanabe S and Matsuzawa M 1993 *Phys. Rev.* A **48** 841
[17] Tang J-Z and Shimamura I 1994 *Phys. Rev.* A **50** 1321
[18] Wintgen D and Delande D 1993 *J. Phys. B: At. Mol. Opt. Phys.* **26** L399
[19] Schulz K, Kaindl G, Domke M, Bozek J D, Heimann P A, Schlachter A S and Rost J M 1996 *Phys. Rev. Lett.* **77** 3086
[20] Menzel A, Frigo S P, Whitfield S B, Caldwell C D, Krause M O, Tang J-Z and Shimamura I 1995 *Phys. Rev. Lett.* **75** 1479
Menzel A, Frigo S P, Whitfield S B, Caldwell C D and M O Krause 1996 *Phys. Rev.* **54** 2080
[21] Fano U 1961 *Phys. Rev.* **124** 1866
[22] Feagin J M and Briggs J S 1988 *Phys. Rev.* A **37** 4599
[23] Rost J M and Briggs J S 1990 *J. Phys. B: At. Mol. Opt. Phys.* **23** L339
[24] Vollweiter A, Rost J M and Briggs J S 1991 *J. Phys. B: At. Mol. Opt. Phys.* **24** L155
[25] Bürgers A, Wintgen D and Rost J M 1995 *J. Phys. B: At. Mol. Opt. Phys.* **28** 3163
[26] Junker B R 1982 *Adv. At. Mol. Phys.* **18** 207
[27] Reinhardt W P 1982 *Ann. Phys. Chem.* **33** 223
[28] Ho Y K 1983 *Phys. Rep.* **99** 1
[29] Seaton M J 1983 *Rep. Prog. Phys.* **46** 167
[30] Hayes M A and Scott M P 1988 *J. Phys. B: At. Mol. Opt. Phys.* **21** 1499
[31] Hamacher P and Hinze J 1989 *J. Phys. B: At. Mol. Opt. Phys.* **22** 3397
[32] Aymar M, Greene C H and Luc-Koenig E 1996 *Rev. Mod. Phys.* **68** 1015
[33] Oza D H 1986 *Phys. Rev.* A **33** 824
[34] Bürgers A and Rost J M 1996 *J. Phys. B: At. Mol. Opt. Phys.* **29** 3825
[35] Friedrich H 1992 *Theoretical Atomic Physics* (Berlin: Springer)
[36] Fano U and Cooper J W 1965 *Phys. Rev.* A **137** 1364
[37] Macek J 1968 *J. Phys. B: At. Mol. Phys.* **1** 831
[38] Lin C D 1983 *Phys. Rev. Lett.* **51** 1348
[39] Tolstikhin O I, Watanabe S and Matsuzawa M 1995 *Phys. Rev. Lett.* **74** 3573
[40] Herrick D R and Sinanoglu A O 1975 *Phys. Rev.* A **11** 97
[41] Cheng-Pan, Starace A F and Greene C H 1994 *J. Phys. B: At. Mol. Opt. Phys.* **27** L137
[42] Kellman M E and Herrick D R 1980 *Phys. Rev.* A **22** 1536
[43] Herrick D R and Kellman M E 1980 *Phys. Rev.* A **21** 418
[44] Herrick D R, Kellman M E and Poliak R D 1980 *Phys. Rev.* A **22** 1517
[45] Leopold J G, Percival I C and Tworkowski A S 1980 *J. Phys. B: At. Mol. Phys.* **13** 1025
[46] Bethe H A and Salpeter E E 1977 *Quantum Mechanics of One- and Two-Electron Atoms* (New York: Plenum)
[47] Slater 1977 *Quantum Theory of Matter* (Huntington: Krieger)
[48] Rost J M, Briggs J S and Feagin J M 1991 *Phys. Rev. Lett.* **66** 1642
Rost J M, Gersbacher R, Richter K, Briggs J S and Wintgen D 1991 *J. Phys. B: At. Mol. Opt. Phys.* **24** 2455
[49] Hunter J E III and Berry R S 1987 *Phys. Rev.* A **36** 3042
[50] Bürgers A and Wintgen D 1994 *J. Phys. B: At. Mol. Opt. Phys.* **27** L131
[51] Blümel R and Reinhardt W P 1995 *Quantum Chaos* ed G Casati and B V Chirikov (Cambridge: Cambridge University Press) p 301
[52] Burgdörfer J, Yang X and Müller J 1995 *Chaos, Solitons Fractals* **5** 1235
[53] Rost J M and Wintgen D 1996 *Europhys. Lett.* **35** 19